HHS Public Access

Author manuscript

Nat Cancer. Author manuscript; available in PMC 2021 September 08.

Published in final edited form as:

Nat Cancer. 2021 February ; 2(2): 218–232. doi:10.1038/s43018-021-00173-0.

Complement activation promoted by the lectin pathway mediates C3aR-dependent sarcoma progression and immunosuppression

Elena Magrini[1], **Sabrina Di Marco**[1], **Sarah N. Mapelli**[1], **Chiara Perucchini**[1], **Fabio Pasqualini**[2], **Alessia Donato**[2], **Maria de la Luz Guevara Lopez**[3], **Roberta Carriero**[1], **Andrea Ponzetta**[1], **Piergiuseppe Colombo**[1], **Ferdinando Cananzi**[1,2], **Domenico Supino**[1,2], **Edimara S. Reis**[4], **Clelia Peano**[1,5], **Antonio Inforzato**[1,2], **Sebastien Jaillon**[1,2], **Andrea Doni**[1], **John D. Lambris**[4], **Alberto Mantovani**[1,2,3,*], **Cecilia Garlanda**[1,2,*]

[1]IRCCS Humanitas Clinical and Research Center, via Manzoni 56, 20089 Rozzano (Milan), Italy

[2]Humanitas University, via Rita Levi Montalcini, 20090 Pieve Emanuele (Milan), Italy

[3]The William Harvey Research Institute, Queen Mary University of London, Charterhouse Square, London EC1M 6BQ.

[4]Department of Pathology and Laboratory Medicine, Perelman School of Medicine, University of Pennsylvania, Philadelphia, Pennsylvania, PA 17 19104, USA.

[5]Institute of Genetic and Biomedical Research, UoS Milan, National Research Council, Rozzano, Milan, Italy

Abstract

Complement has emerged as a component of tumor promoting inflammation. We conducted a systematic assessment of the role of complement activation and effector pathways in sarcomas. *C3*$^{-/-}$, *MBL1/2*$^{-/-}$ and *C4*$^{-/-}$ mice showed reduced susceptibility to 3-methylcholanthrene sarcomagenesis and transplanted sarcomas, whereas C1q and factor B deficiency had marginal effects. Complement 3a receptor (C3aR), but not C5aR1 and C5aR2, deficiency mirrored the phenotype of *C3*$^{-/-}$ mice. C3 and C3aR deficiency were associated with reduced accumulation and functional skewing of tumor-associated macrophages, increased T cell activation and response to anti-PD-1 therapy. Transcriptional profiling of sarcoma infiltrating macrophages and monocytes revealed the enrichment of MHC II-dependent antigen presentation pathway in C3-deficient cells. In patients, C3aR expression correlated with a macrophage population signature and C3

*Corresponding authors: A.M. (alberto.mantovani@humanitasresearch.it) and C.G. (cecilia.garlanda@humanitasresearch.it).

Author Contributions

E.M. designed and conducted the experiments and drafted the manuscript. S.D.M. contributed to *in vitro* and *in vivo* experiments. C.Perucchini, M.G.L., A.P. and D.S. provided technological support in *in vivo* experiments. F.P., P.C. and F.C. contributed to histological analysis. C.Peano performed the preparation of samples for RNAseq analysis. S.N.M., A.Donato. and R.C. analysed RNAseq and human TCGA data. A.I., S.J. and A.Doni contributed to the experimental design and data analysis. E.S.R. and J.D.L. provided gene-targeted animals and contributed to the experimental design and data analysis. A.M. and C.G. contributed to the experimental design, the supervision of the study, wrote and revised the manuscript.

Declaration of interests

The authors except J.D.L. declare no competing financial interests. J.D.L. is the founder of Amyndas Pharmaceuticals, which is developing complement inhibitors for therapeutic purposes, is the inventor of patents or patent applications that describe the use of complement inhibitors for therapeutic purposes, some of which are developed by Amyndas Pharmaceuticals. J.D.L. is also the inventor of the compstatin technology licensed to Apellis Pharmaceuticals [i.e., 4(1MeW)7W/POT-4/APL-1 and PEGylated derivatives such as APL-2/pegcetacoplan].

deficiency-associated signatures predicted better clinical outcome. These results suggest that the lectin pathway and C3a/C3aR axis are key components of complement and macrophage-mediated sarcoma promotion and immunosuppression.

Keywords

Complement; lectin pathway; mannose binding lectin (MBL); C3; C3a receptor (C3aR); cancer; sarcoma; cancer-related inflammation; macrophages; immunotherapy

The tumor microenvironment comprises inflammatory cells and mediators which contribute to tumor-promoting mechanisms [1,2,3]. In addition to being part of the tumor microenvironment, chronic inflammation may mediate tumor initiation and promote genetic instability. A central role in cancer-related inflammation is played by cells of the monocyte-macrophage lineage, which engage in complex interactions with cancer cells, as well as stromal and tumor immune infiltrating cells, promoting cancer cell proliferation and survival, angiogenesis, and suppressing anti-tumor T cell responses [4,5]. Several factors, including hypoxia, chemokines and cytokines and metabolic products of cancer cells (e.g., lactic acid) are involved in tumor-associated macrophage (TAM) recruitment and functional skewing [5,6].

The humoral innate immunity comprises diverse molecules including the complement system, collectins, ficolins, and pentraxins [7]. Historically considered an anti-tumor system, complement can exert dual roles in cancer as it may activate anti- and pro-tumor mechanisms [8,9]. It plays a role as an effector mechanism of complement-dependent cytotoxicity and phagocytosis induced by therapeutic monoclonal antibodies against hematopoietic tumors [10,11]. In addition, complement anaphylatoxins are mediators of radiotherapy-induced tumor-specific immunity [12]. On the other hand, several cell types in the tumor microenvironment are both a source and a target of complement products [8,13,14,15,16]. In particular, anaphylatoxin receptors can be expressed by lymphocytes, myeloid cells, cancer cells, and influence their functions [15]. For instance, C5a enhanced the growth of a transplanted tumor by recruiting myeloid-derived suppressor cells and amplifying their T cell suppressive properties [17,18] or directly favored tumor cell proliferation and invasiveness [19].

C3 gene targeting has provided unequivocal genetic evidence that components of the complement cascade can promote carcinogenesis in mice [17,20,21]. Moreover, evidence in mice and humans suggests that a regulator of the complement cascade, PTX3, can act as an extrinsic oncosuppressor in murine sarcomagenesis and in selected tumors [21,22].

The present study was designed to conduct a systematic assessment of complement activation and effector pathways in carcinogenesis. In primary 3-methylcholanthrene (3-MCA) sarcomagenesis and two transplanted mouse sarcomas, the lectin pathway and the C3a receptor (C3aR) emerged as important components of tumor promotion, driving macrophage recruitment and skewing, immunosuppression and resistance to anti-PD-1 immunotherapy. In human sarcomas, C3 deficiency-associated transcriptional signatures were found to correlate with better prognosis.

Results

Role of complement activation and effector pathways in primary sarcomagenesis and transplanted sarcomas

In a first set of experiments (n=14 with 8 complement-deficient strains) we explored the role of complement deficiency in 3-MCA-induced sarcomagenesis (Fig. 1, Extended Data Fig. 1). In agreement with previous results obtained in C3-deficient *vs* competent littermates [21], C3 genetic deficiency was associated with delayed tumor appearance (Fig. 1a). MBL1/2 deficiency was associated with reduced primary sarcoma incidence (85% $MBL1/2^{-/-}$ mice developed tumor 150 days after 3-MCA injection compared to 100% wt mice, p=0.001) (Fig. 1b). C4 deficiency closely mimicked the phenotype of $C3^{-/-}$ and $MBL1/2^{-/-}$ mice (Fig. 1c). The classical and alternative pathways were irrelevant since $C1q^{-/-}$ and $fB^{-/-}$ mice showed no ($C1q^{-/-}$) or little ($fB^{-/-}$) protection compared to wt mice (Fig. 1d–e). These results suggest that in primary 3-MCA-induced sarcomagenesis the lectin pathway plays a dominant role in complement dependent tumor promotion, with the classic and alternative pathways having no significant impact.

Moving downstream in the complement cascade, we assessed 3-MCA sarcomagenesis in $C5aR1^{-/-}$, $C5aR2^{-/-}$ and $C3aR^{-/-}$ mice (Fig. 1f–h). In transplanted, genetic and carcinogen-induced tumor models C5a has been reported to drive recruitment of myeloid cells, tumor growth and metastasis [8,15,23]. Here, C5aR1 and C5aR2 deficiency had no impact on susceptibility to 3-MCA sarcomagenesis (Fig. 1f–g). In contrast, $C3aR^{-/-}$ mice showed delayed appearance of 3-MCA sarcomas (81% $C3aR^{-/-}$ mice developed tumor 187 days after carcinogen injection compared to 100% wt mice, p<0.0001) (Fig. 1h), mirroring the phenotype of $MBL1/2^{-/-}$, $C3^{-/-}$ and $C4^{-/-}$ mice. These results suggest that downstream of complement activation, C3a and its cognate receptor C3aR are the main effector molecules involved in complement-mediated amplification of sarcoma promotion.

The subcutaneous 3-MCA-induced sarcomas is considered to represent the counterpart of undifferentiated pleomorphic sarcoma (UPS) [24,25,26]. Despite reduced tumor growth in complement-deficient mice, MBL1/2, C4, C3 or C3aR deficiency did not affect the histology characteristics of 3-MCA-induced sarcomas (Extended Data Fig. 1).

To dissect the mechanism underlying the role of complement in sarcoma promotion, two subcutaneously transplanted tumor models were used (Fig. 2). Growth of the MN/MCA1 and FS6 sarcomas were remarkably reduced in C3- and C4-deficient hosts (Fig. 2a–d). In contrast C1q and factor B deficiency had little ($C1q^{-/-}$) or no ($fB^{-/-}$) impact on growth of these two sarcomas (Fig. 2e–h). MBL1/2 deficiency was associated with remarkable protection against the FS6 sarcoma, whereas it had a minor impact on MN/MCA1 (Fig. 2i–j). In addition, C3aR deficiency (Fig. 2k–l), but not C5aR1 or C5aR2 deficiency (Fig. 2m–p), conferred resistance to MN/MCA1 and FS6 growth. The experiments shown in Fig. 2e and 2k were performed using C1q- or C3aR-deficient mice co-housed with wt and heterozygous littermates, thus suggesting that the microbiome was not involved in the phenotype. Whereas in the MN/MCA1 model the incidence was 100% in every strain, in the non-metastatic FS6 sarcoma, genetic deficiency in selected complement components was associated with a substantial number of mice rejecting the tumor transplant [38%

C3$^{-/-}$, 22% *MBL1/2*$^{-/-}$, 60% *C4*$^{-/-}$ and 58% *C3aR*$^{-/-}$ mice developed tumors compared to 80–93% wt mice, (p=0.004; p=0.008; p=0.004; p=0.004, respectively)] (Extended Data Fig. 1). FS6 sarcoma growth and incidence were significantly reduced in *MBL1/2*$^{-/-}$ and *C3aR*$^{-/-}$ mice compared to heterozygous littermates (Extended Data Fig. 1). In the aggressive MN/MCA1 sarcoma [27], C3 deficiency was also associated with reduced secondary metastatic dissemination after im injection (Fig. 2q). Compared to primary 3-MCA sarcomagenesis (Fig. 1b), other glycan-recognising soluble pattern recognition molecules may be responsible for triggering the complement cascade in the MN/MCA1 sarcoma. Collectively the results obtained in two transplantable sarcomas confirm the role of complement components in tumor progression observed in primary sarcomagenesis, extend their significance to metastasis and highlight the key role of C3aR.

Complement deposition *in vivo* and *in vitro*

Local activation of C3 was previously observed in 3-MCA primary sarcomagenesis, at the injection site and in established tumors [21]. To investigate complement activation in transplantable sarcomas, we analysed the deposition of C3 cleavage products (C3b, iC3b, C3c) in MN/MCA1 tumors by immunofluorescence (Fig. 3a–b). Confocal microscopy showed that C3 deposition occurred in selected areas of the tumor on cancer cells, and on CD31^{+} vascular cells, but not on CD45^{+} leukocytes (Fig. 3a). In addition, C3a and C5a were localized *in situ* produced both in chemically induced [21 and not shown] and MN/MCA1 transplantable sarcoma and increased during tumor growth (e.g. C3a: 1.86 ± 0.34 ng/mg total proteins at 14 days compared to 4.94 ± 1.06 ng/mg total proteins at 21 days, p=0.036) (Fig. 3c–d).

To further dissect the mechanisms of C3 activation in sarcoma, C3 deposition on sarcoma cells was also investigated *in vitro* by flow cytometry. C3 cleavage products were detected on 3-MCA derived sarcoma cells, FS6 and MN/MCA1 cells after incubation with fresh but not heat-inactivated serum (Fig. 3e). C3 cleavage products were not detected on cells derived from peritoneal washes of wt mice (Extended Data Fig. 2), in agreement with *in vivo* observations on the lack of C3 deposition on immune cells (Fig. 3a). To assess the involvement of glycosylation in complement activation, the C3 deposition assay was performed with sarcoma cells pre-treated with tunicamycin, an inhibitor of protein N-glycosylation. Treatment with tunicamycin effectively reduced the binding to tumor cells of DSA, GNA, MAA and SNA lectins, which recognize terminal residues of galactose, mannose, α-(2➔3) sialic acid, and α-(2➔6) sialic acid, respectively (Extended Data Fig.2), and significantly reduced the deposition of C3 cleavage products on 3-MCA derived sarcoma cells (p=0.032), FS6 (p=0.004) and MN/MCA1 cells (p=0.005) (Fig. 3f).

To investigate which activation pathway was involved, the C3 deposition assay was performed with serum collected from wt or complement deficient mice. The deposition of C3 cleavage products on 3-MCA derived and MN/MCA1 sarcoma cells was significantly reduced in presence of serum collected from *MBL1/2*$^{-/-}$, *C1q*$^{-/-}$ and *C4*$^{-/-}$ but not *fB*$^{-/-}$ mice (Extended Data Fig.2).

These results indicate that C3 activation occurs on sarcoma cells *in vitro*, and recognition of aberrant glycosylation patterns on tumor cells by the classical or lectin pathways is involved in complement activation.

Role of C3 and C3aR in macrophage recruitment and skewing

To identify the C3a targets in sarcomas, we analysed mRNA expression of C3aR in MN/MCA1 or 3-MCA derived tumor cells and tumor infiltrating leukocytes (Fig. 4a). The C3aR mRNA was mainly expressed by tumor infiltrating macrophages, monocytes, neutrophils, and to lower extent, by T cells. In contrast, no or very low C3aR expression was observed in MN/MCA1 or 3-MCA derived tumor cells (Fig. 4a), suggesting that a direct effect of C3a complement activation fragment on tumor cells was unlikely. The absence of C3aR protein in sarcoma cells and its expression in peritoneal macrophages (Fig. 4b) or activated (Iba-1$^+$) tumor infiltrating macrophages (Fig. 4c) was confirmed by immunofluorescence.

Because of its aggressiveness and metastatic behavior the MN/MCA1 sarcoma model was selected for further mechanistic analysis. Based on C3aR expression data, we focused on TAMs. A significant reduction of macrophages (34% ± 2.2% in *C3*$^{-/-}$ compared to 40% ± 1.4% in wt mice, p=0.036; 21% ± 4.4% in *C3aR*$^{-/-}$ compared to 40% ± 2.6% in wt mice, p=0.006) was observed in both *C3*$^{-/-}$ and *C3aR*$^{-/-}$ compared to wt MN/MCA1 tumor bearing mice (Fig. 4d). In contrast, increased frequency of Ly6C$^+$ monocytes was detected in *C3*$^{-/-}$ (not significant) and *C3aR*$^{-/-}$ (p=0.002) tumors (Fig. 4e, Extended Data Fig. 3). We previously showed that deregulated complement activation in PTX3-deficient 3-MCA sarcoma was responsible of macrophage M2-like polarization [21]. Thus, we characterized the phenotype of TAMs infiltrating MN/MCA1 tumors by flow cytometry and observed a reduced frequency of CD206$^+$ (an M2-like marker) TAMs in C3-deficient mice compared to wt (Fig. 4f) and upregulation of M1-like markers (CD11c, MHC II, CD80, CD86) (Fig. 4g). Similar results in terms of CD206$^+$ TAM frequency and skewing were observed in C3aR-deficient MN/MCA1 tumors analysed 21 days after transplant (Fig. 4h–i). To exclude an effect of tumor volume on TAM frequency and skewing, we analysed wt and C3aR-deficient tumors with the same volume (2 cm^3). Also in this case C3aR deficiency was associated with significantly decreased macrophage infiltrate in tumors, increased monocyte abundance, and upregulation of CD11c, MHC II, CD80, CD86 (Fig. 4j–l). Reduced TAM frequency and skewing toward a M1-like phenotype were confirmed in MN/MCA1 tumors of im injected *C3*$^{-/-}$ mice and in FS6 tumors of *C3aR*$^{-/-}$ mice (Extended Data Fig. 4). Increased CD11c or MHC II expression was confirmed in TAMs collected from 3-MCA-induced 4 sarcoma bearing *C3*$^{-/-}$ mice, compared to wt (not shown).

Finally, since M2-like macrophages sustain tumor angiogenesis, we analysed the vasculature in wt and *C3*$^{-/-}$ tumors. The analysis revealed no difference in terms of vessel density, vascular area and vessel stability, measured as pericyte coverage (Extended Data Fig. 4), indicating that regulation of angiogenesis was not involved in the phenotype of *C3*$^{-/-}$ mice.

Transcriptional profiling of C3-deficient sarcoma infiltrating leukocytes

To obtain a deeper insight into the impact of C3 deficiency on TAM functional activation, RNA sequencing (RNA-seq) analysis was conducted on FACS-sorted MN/MCA1-infiltrating macrophages and monocytes.

Clustering and principal component analyses on transcriptional data showed that the expression of the top 1000 most variable genes was sufficient to correctly identify the two different populations (as most prominent feature) (Fig. 5a–b, Extended Data Fig. 5) and in a subsequent instance, to separate samples based on the diverse genotypes (Extended Data Fig. 5), which results as major cause of variance in PCA analyses in individual population (Fig. 5c–d). Perturbation of gene expression associated with C3 deficiency resulted in 8% of the overall variance across all biological samples and replicates, as identified by the second principal component (Extended Data Fig. 5).

In order to gain insights on the effect of C3 deficiency on the transcriptional profile of the two cell populations, deregulated genes were extracted. Differential expression methods were applied to identify differences in quantified gene counts representing the transcriptional change that each infiltrating cell population undergoes. The comparisons resulted in the selection of 297 (Extended Data Fig. 5, Supplementary Tables 1, 2) differentially expressed genes in macrophages and monocytes in the two genotypes.

Among the differentially expressed genes in C3-deficient compared to wt cells, several were involved in MHC II-dependent antigen presentation (Fig. 5e–f). This finding was also confirmed with pre-ranked gene set enrichment analysis, which enlightened the gene ontology “MHC class II protein complex” pathway to be enriched in genes upregulated in macrophages and monocytes from C3-deficient hosts (Supplementary Tables 3, 4). Similar indications were obtained by Ingenuity Pathway Analysis (IPA) software, which pinpointed the centrality of antigen presentation in $C3^{-/-}$ *vs* wt mice (Fig. 5g–h).

Among the genes constituting the “MHC class II biological process”, Ciita encoding Class II transactivator (CIITA) was highly increased in macrophages and monocytes from C3-deficient hosts (Fig. 5i, Supplementary Tables 1–2, 5–6).

Among upregulated genes in macrophages and monocytes from C3-deficient hosts, we also found chemokines involved in T cell recruitment and activation (cxcl13, cxcl11) or in B cell recruitment (cxcl13), scavenger receptors (siglec/CD209, clec4b1), chemokine receptors involved in myeloid cell recruitment and activation (ccr4, ccr3), molecules associated with myeloid cell activation and type 1 responses (CD83, socs1, irf1) (Fig. 5e–h, Supplementary Tables 1–2).

Collectively these results suggest that C3 deficiency was associated with gene expression reprogramming in tumor infiltrating leukocytes leading to increased antigen presentation.

Role of C3 and C3aR in T cell recruitment and function and *in vivo* relevance

We next investigated whether C3 and C3aR deficiency impacted on T cell-dependent anti-tumor effector mechanisms. The frequency of MN/MCA1 tumor infiltrating $CD4^+$ T

lymphocytes was significantly increased in C3aR-deficient mice and a similar trend was also observed in C3-deficient mice (Fig. 6a, Extended Data Fig. 6). Gene expression analysis of $CD4^+$ T cells sorted from C3-deficient mice showed significantly higher expression of Th1 markers such as *Tbet, Eomes, Ifng* (Fig. 6b). Higher Tbet and Eomes expression in C3-deficient $CD4^+$ cells was validated by FACS analysis (Fig. 6c) and confirmed in C3aR-deficient $CD4^+$ cells (Fig. 6d).

C3 and C3aR deficiency were also associated with increased frequency of $CD8^+$ tumor infiltrating T cells (2.1% ± 0.3% in $C3^{-/-}$ compared to 0.9% ± 0.1% in wt mice, p=0.001; 4% ± 1% in $C3aR^{-/-}$ compared to 1.5% ± 0.1% in wt mice, p=0.039) (Fig. 6e) and in particular of $CD44^+CD62L^-CD8^+$ cells (1.5% ± 0.3% in $C3^{-/-}$ compared to 0.6% ± 0.08% in wt mice, p=0.015; 1.9% in $C3aR^{-/-}$ compared to 0.9% in wt mice, p=0.009) (Fig. 6f, Extended Data Fig. 6), which constitute the activated effector or effector memory subtypes. Increased frequency of $CD4^+$ and $CD8^+$ T cells and of $CD44^+CD62L^-CD8^+$ cells was also observed in C3aR-deficient tumors analysed at equal volume (2 cm^3) (Fig. 6g), indicating that the difference observed 21 days after tumor injection did not depend on tumor volume. These results were confirmed in FS6 tumors (Extended Data Fig. 4). In addition, IFNγ levels were higher in C3- and C3aR-deficient tumor lysates compared to wt (4.3 ± 0.47 pg/mg and 4.8 ± 0.64 pg/mg total proteins in C3- and C3aR-deficient tumors, compared to 2.7 ± 0.25 pg/mg total proteins in wt tumors, p=0.003 and p=0.001, respectively) (Fig. 6h).

The depletion of $CD8^+$ T cells significantly increased MN/MCA1 tumor growth in $C3^{-/-}$ mice but did not modify the tumor growth in wt mice (Fig. 6i), thus indicating that $CD8^+$ T cells played anti-tumor activity in $C3^{-/-}$ mice, but were suppressed in wt mice. Finally, IFNγ blockade significantly increased the tumor growth in C3-deficient mice as well as in wt mice (Fig. 6j), suggesting that $CD8^+$ cells and IFNγ were involved in the effector mechanisms underlying the phenotype of $C3^{-/-}$ mice.

These results indicated that C3 and C3aR deficiency dependent tumor resistance was associated with increased Th1 responses and effector potential of $CD8^+$ T cells. We thus investigated whether C3- or C3aR deficiency affected the efficacy of checkpoint blockade immunotherapy. The treatment of wt mice with anti-PD-1 monoclonal antibody (RMP1-14 clone) had marginal effects in the MN/MCA1 subcutaneous sarcoma model in wt mice, whereas the treatment of C3-deficient mice resulted in a significant reduction of primary tumor growth compared to anti-PD-1 treatment or C3 deficiency alone (Fig. 6k). In addition, in the metastatic MN/MCA1 sarcoma model, lung metastases were almost abrogated upon combination of C3 deficiency with anti-PD-1 treatment and were significantly reduced compared to anti-PD-1 treatment or C3 deficiency alone (Fig. 6l). These results demonstrate that C3 deficiency increased the efficacy of anti-PD-1 treatment both in primary tumor growth and secondary metastases, suggesting that the absence of complement activation generated a tumor microenvironment more favorable to response to immunotherapy.

To investigate the translational implications of these results, we finally assessed whether pharmacological inhibition of C3aR affected the efficacy of checkpoint blockade immunotherapy. We performed experiments of MN/MCA1 (Fig. 6m) and FS6 (Fig. 6n) sarcomas in wt mice treated with SB 290157 trifluoroacetate salt, a C3aR antagonist

(C3aRa), in combination with anti-PD-1 treatments. The combination resulted in a significant reduction of primary tumor growth compared to anti-PD-1 or C3aRa treatment alone both in terms of tumor growth and incidence (Fig. 6m–n), indicating an additive (in MN/MCA1) or synergistic (in FS6) effect.

C3 deficiency signatures are associated with survival of human sarcoma patients

In an effort to obtain indications as the relevance in humans of results obtained in mouse models, we interrogated public databases of RNA-seq data derived from human sarcomas available in The Cancer Genome Atlas (TCGA) cohort [28]. We first analyzed mRNA expression of C3 and other complement genes, but we did not find any correlation with outcome (not shown), in agreement with previous analysis [9]. Then, considering that the main source of complement molecules may be systemic and not local, we evaluated complement activation-associated signatures in macrophages and monocytes. To this aim, we performed a differential expression analysis comparing all genotypes and replicates of mouse macrophages *vs* monocytes (Supplementary Table 7), in order to identify modules of human orthologue genes able to distinguish the two individual sorted cell populations (Supplementary Tables 8–9). These extracted gene panels were therefore considered surrogate signatures able to represent the examined tumor infiltrating cell types. We observed a positive correlation between C3AR1 expression levels and macrophage or monocyte quantification scores (Fig. 7a–b). These results indicated that, in agreement with evidence obtained in mice (Fig. 4d), C3aR correlates with and reflects macrophage infiltration (Fig. 7a).

Then, we asked whether upregulated genes in C3-deficient macrophages and monocytes were able to predict overall survival (OS), supporting the hypothesis of a protumoral role of complement activation in these malignancies. We extracted the positively differentially expressed genes of C3-deficient mouse macrophages and monocytes (Supplementary Tables 1–2) and generated two signatures of human orthologue genes (Extended Data Fig. 5, Supplementary Table 10). Then, we built a computational model, which combined C3 deficiency- and cell population-associated signatures, and generated for each patient a single score representing the analogy to C3-deficient profile normalized on the estimated abundance of cell infiltration. Survival analyses indicated that patients exhibiting higher expression of C3 deficiency-associated signatures had a better prognosis, in terms of OS (Fig. 7c–d).

Moreover, C3-deficiency associated signatures of macrophages and monocytes significantly correlated with an M1-like macrophage signature (obtained by CIBERSORT) [29] (Fig. 7e–f).

Finally, complement C1q, C4d and C3c deposition and C3aR expression were validated by immunohistochemistry in a separate cohort of 19 UPS patients followed at Humanitas Clinical and Research Center (Extended Data Fig. 7). C3aR immunoreactivity was detected in 14/19 samples and was mostly confined to infiltrating macrophages (Extended Data Fig. 7). Disease-free survival (DFS) and metastasis-free survival were higher in $C3aR^{neg}$ (Mean immunoreactive area - IRA - per patient: 0%) compared to $C3aR^{pos}$ (Mean IRA per patient: range 0.64% - 20.95%) UPS patients (Extended Data Fig. 7), indicating that

C3aR-expression contributed to sarcoma aggressiveness and spreading, mirroring findings observed in mouse models.

Discussion

The present study was designed to conduct a systematic analysis of complement activation and effector pathways in a classic model of primary 3-MCA-induced sarcomagenesis, prompted by a previous investigation in *C3*$^{-/-}$ and *PTX3*$^{-/-}$ mice [21], as well as in different transplantable sarcoma models. The results reported here confirm and extend previous observations on complement mediated tumor promotion [8,14,17,18,30,31,32,33,34,35,36,37] and reveal underlying mechanisms, by highlighting a role of the lectin pathway and of C3aR.

In this study several sarcoma models were used in an effort to conduct a systematic analysis. The subcutaneous 3-MCA-induced sarcoma mimics the undifferentiated pleomorphic sarcoma (UPS) [24,25,26] and has the advantage of representing the entire process of tumor progression and immunoediting, whereas the transplantable sarcoma models more likely mimic the clinical situation, characterized by the presence of an established tumor, frequently showing a high growth rate. Subcutaneous injection of 3-MCA or sarcoma cell lines induces primary sarcomas with different growth rate, that are not associated with secondary metastatic dissemination, whereas the im injection of the MN/MCA1 line generates lung metastasis. In all these models we could observe complement-mediated tumor promotion.

In primary 3-MCA sarcomagenesis and in one transplanted sarcoma MBL1/2 deficiency accounted for complement mediated tumor promotion. Previous studies showed that the classical pathway was responsible for complement activation in a murine model of cervical cancer [17,20] and in human clear-cell renal cell carcinoma [20]. In a genetic mouse model of primary epithelial carcinogenesis driven by immune complexes, Fcγ receptors rather than the classic complement activation pathway were involved [38]. In the same model, complement activation was driven by urokinase (uPA)$^{+}$ macrophages regulating C3-independent release of C5a during premalignant progression [39]. In a chemically-induced skin cancer model, the alternative pathway was shown to promote tumor growth [40]. In a recent study, pathogenic fungi were shown to promote pancreatic ductal adenocarcinoma (PDAC) by triggering MBL-dependent complement activation [41]. In the present study activation of the lectin pathway was associated with direct glycosylation-dependent interaction with sarcoma cells. This finding may reflect altered glycosylation associated with sarcomagenesis [8,42].

Thus, complement activation and effector pathways involved in tumor-promoting inflammation differ in different models including primary carcinogenesis in different organs (present study; [39,41]). In a predictive/intervention perspective, it will be important to assess the relative importance of complement components in different human tumors.

Complement activation in cancer was associated with skewing of myeloid cell function and T cell immunosuppression. The complement activation fragments C5a and C3a represent a major effector pathway downstream of complement activation. Several studies reported that

C5a and C3a induce the production of chemokines including MCP-1/CCL2 in leukocytes, such as macrophages [43,44] and mast cells [45], through an AKT-dependent pathway. CCL2 is a major inducer of M2-like macrophage skewing [46,47]. In a number of reports C5a has emerged as a driver of recruitment and skewing of myeloid cells in cancer [8]. In a model of squamous carcinogenesis, C5a was shown to regulate protumorigenic properties of $C5aR1^+$ mast cells and macrophages [39]. C3a has been suggested to promote carcinogenesis by affecting neutrophil recruitment and $CD4^+$ T cell activation in a melanoma transplanted model [33], activating protumorigenic neutrophils in small intestinal tumorigenesis [32], promoting leptomeningeal metastasis by disrupting the blood-cerebrospinal fluid barrier [36] or directly inducing PI3K/AKT-dependent tumor cell proliferation and epithelial-mesenchymal transition [30,48]. The results reported here provide strong genetic evidence that in primary 3-MCA sarcomagenesis and in two transplanted sarcoma models the C3a/C3aR axis plays a dominant role in TAM recruitment and functional skewing, driving immunosuppression and tumor promotion. Thus, the complement system has a crucial role in sarcoma progression and C3a in particular acts as an important element in the orchestration of an immunosuppressive tumor microenvironment in sarcomagenesis and may represent a therapeutic target.

Several lines of evidence suggest that the complement cascade plays a role in human cancer [8,15]. The complement regulator PTX3 has been shown to act as an extrinsic oncosuppressor, epigenetically silenced in selected human tumors [21,22]. In human clear-cell renal cell carcinoma patients, tumors highly infiltrated by C1q-producing TAMs exhibited an immunosuppressed microenvironment, characterized by high expression of immune checkpoints (i.e., PD-1, Lag-3, PD-L1, PD-L2), suggesting a correlation between complement activation and T cell exhaustion [20]. In preclinical models, the combination of anti-PD-1 and anti-C5a drugs has been proposed as a novel therapeutic strategy for lung cancer [37]. The results presented here indicate that in sarcoma C3- and C3aR deficiency were associated with type 1 skewing of $CD4^+$ T cells, increased frequency of effector $CD8^+$ T cells and higher IFNγ levels, and potentiated the effect of anti-PD-1-dependent immunotherapy. Interestingly from a translational perspective, the pharmacological inhibition of C3aR was sufficient to potentiate anti-PD-1 therapy. Sarcomas represent a heterogeneous group of cancer, comprising several histological subtypes and exhibiting different responses to immune-checkpoint blockade-based therapy. Recently, a new classification of soft-tissue sarcomas revealed an association between the composition of the tumor microenvironment and response to PD-1 blockade [49]. In particular, B cells were shown to be associated with survival and immunotherapy response in sarcoma [49]. Our data show that C3-deficiency was associated with increased expression of Cxcl13, a B cell recruiting chemokine, in sarcoma-infiltrating macrophages and monocytes, and further support the hypothesis that combination of complement targeting strategies with immunotherapeutic treatments would reduce resistance to immunotherapy in selected sarcoma patients.

In three mouse strains (C3aR-, MBL- and C1q-deficient mice) and two transplantable models (MN/MCA1 and FS6) heterozygous mice showed higher incidence or tumor volume compared to homozygous deficient mice, indicating that the phenotypes observed when complement-deficient mice were compared to commercial wt mice, were not due to

differences in the genetic background, but to complement-deficiency. In 3-MCA-induced primary carcinogenesis, wt littermates were compared to C3-deficient mice [21], but not to C4-, MBL1/2-, C4- or C3aR-deficient mice. Thus, the irrelevance of the genetic background of these strains in the phenotypes observed cannot be formally excluded.

The results presented here using genetic approaches and primary sarcomagenesis show that the complement lectin pathway is an important player in the orchestration of tumor promotion. The impact on sarcomagenesis was associated with glycan recognition on sarcoma cells. Co-housing experiments suggest that the phenotype was microbiome independent. In contrast, in a model of PDAC pathogenic fungi recognized by MBLs lead to complement activation in tumor tissue [41]. In other transplanted or genetic tumor models complement activation proceeds through the classical pathway [17,20] or can be due to C3-independent release of C5a [39]. Thus, in different tissue and/or tumor contextures complement can contribute to tumor progression via different activation pathways. In this general perspective, an unexpected consistent finding observed in the present study was the essential role of the C3aR as an effector of complement activation that mediated immunosuppression and sarcoma promotion. In addition, we highlight the possibility of evaluating the protumoral role of complement activation even in those tumors in which complement genes are not up-regulated from a transcriptional point of view [9], considering that the source of production of these proteins is not necessarily local. In a translational perspective, the role of complement-mediated tumor promotion needs to be dissected in different tumor contexts and C3 targeting and C3aR inhibition represent a promising therapeutic avenue in particular in combination with checkpoint blockade immunotherapy.

Methods

Animals

Cancer models were performed in 8–13 weeks-old male mice. Wild type (wt) mice on a C57BL/6J genetic background were purchased from Charles River Laboratories, Calco, Italy. Mice deficient for C1q, C4b, MBL1/2, C3, C3aR, C5aR1 and C5aR2 ($C1q^{-/-}$, $C4b^{-/-}$, $MBL1/2^{-/-}$, $C3^{-/-}$, $C3aR^{-/-}$, $C5aR1^{-/-}$ *and* $C5aR2^{-/-}$) were on a C57BL/6J genetic background, factor B-deficient mice ($fB^{-/-}$) were on a C57BL/6NJ genetic background. When specified, co-housed wt or heterozygous littermates were used.

$C1q^{-/-}$, $C4b^{-/-}$, $C5aR1^{-/-}$ and $C5aR2^{-/-}$ were provided by J.D. Lambris. $C3aR^{-/-}$ were provided by H.F. Langer, University of Tübingen, Germany. $C3^{-/-}$, $MBL1/2^{-/-}$, $fB^{-/-}$ and wt mice on a C57BL6/NJ background were purchased from The Jackson Lab (Bar Harbor ME, US). All colonies were bred by Charles River Laboratories, Calco, Italy, and then used in the Humanitas SPF animal facility in individually ventilated cages. Procedures involving animals handling and care were conformed to protocols approved by the Humanitas Clinical and Research Center in compliance with national (D.L. N.116, G.U., suppl. 40, 18–2-1992 and N.26, G.U. March 4, 2014) and international law and policies (EEC Council Directive 2010/63/EU, OJ L 276/33, 22–09-2010; National Institutes of Health Guide for the Care and Use of Laboratory Animals, US National Research Council, 2011). The study was approved by the Italian Ministry of Health (approval n. 122/2016-PR, issued on 05/02/2016). All efforts were made to minimize the number of animals used and their suffering.

Sarcoma models

Chemically induced sarcomagenesis was induced as previously described [21]. Briefly, mice were injected sc on the back with a single dose of 100 μg of 3-MCA (Sigma-Aldrich, St Louis, US) dissolved in corn oil (1 mg/ml) and assessed for sarcoma development once/week over the course of 5–6 months. For the transplantable C57BL/6 sarcoma models, mice were injected with mycoplasma-free MN/MCA1 cells (5×10^5/100 μl PBS sc on the back or 10^5/100 μl PBS im in the thigh) or FS6 cells (2×10^6/100 μl PBS sc), [24,27]. Tumor growth was measured twice/week and mice were euthanized 21 or 27 and 32–36 days later, respectively. In the MN/MCA1 im model, lung metastases were assessed by macroscopic counting by a blinded observer at the time of being euthanized 27 days after injection, as previously described [27]. MN/MCA1 and FS6 cells were authenticated morphologically by microscopy *in vitro* and by histology *ex vivo*. Data are shown as tumor incidence and tumor volume, measured with a caliper, calculated according to the formula: Volume = $(D\times d^2)/2$, where D = larger tumor diameter and d = smaller tumor diameter.

Depletion and blocking experiments

Mice were treated ip with 200 μg of specific mAbs (*InVivo*Plus anti-mouse CD8, clone YTS169.4 and isotype control Rat IgG2b, clone LTF2; *InVivo*Mab anti-mouse IFNγ, clone XMG1.2 and isotype control Rat IgG1, clone HRPN; all from BioXCell, West Lebanon, US) the day before tumor injection and then with 100 μg twice (anti-CD8) or three times/week (anti-IFNγ) for the entire duration of the experiment. When specified, mice were treated ip twice/week with 200 μg of anti-mouse PD-1 (clone RMP1-14) or relative Rat IgG2a isotype control (clone 2A3), (*InVivo*Plus, BioXCell), starting from 5 days after tumor cell injection, and with the C3aRa SB 290157 trifluoroacetate salt (Santa Cruz, 5mg/Kg ip) three (MN/MCA1) or six (FS6) times/week, or vehicle.

FACS analysis

Single-cell suspension were obtained by mechanical and enzymatic dissociation in 0.1 mg/ml Type IV Collagenase (Sigma Aldrich) for 1h at +37°C. Cell viability was determined by Aqua LIVE/Dead Fixable-405nm staining (Invitrogen, Carlsbad, US). Cells were then incubated with 20 μl of Fc block reagent (purified anti-CD16/32, clone 93, eBioscience – ThermoFisher, Waltham, US). 50 μl of a mix of antibodies diluted in FACS buffer was added to each sample. The following murine antibodies were used: anti-CD45-BV605 (clone 30-F11; 0.5 μl); anti-CD11b-BV786 or -APC-Cy7 (clone M1/70; 0.25 or 0.15 μl, respectively); anti-CD11c-AF700 (clone HL3; 1 μl); anti-Ly6C-FITC or -BV421 (clone AL-21; both 0.25 μl); anti-F4/80-PeCy7 (clone BM8; 1 μl); anti-Ly6G-PECF594 (clone 1A8; 0.25 μl); anti-NK1.1-PECF594 (clone PK136; 0.6 μl); anti-CD19-APC or -eF450 (clone 1D3; 0.5 μl or 1 μl, respectively); anti-CD80-PerCP-Cy5.5 (clone 16-10A1; 1 μl); anti-CD86-eF450 (clone GL-1; 1 μl); anti-CD206-APC (clone C068C2; 0.5 μl); anti-CD3-PerCP-Cy5.5 (clone 145-2C11; 1 μl); anti-CD4-AF700 or –FITC (clone RM4-5; both 1 μl); anti-CD8a-PE or –BV480 (clone 53-6.7; 0.25 μl or 0.3 μl, respectively); anti-MHCII-FITC, -PE or- BV711 (clone M5/114.15.2 or 2G9; 0.4 μl, 0.25 μl or 0.25 μl, respectively); anti-TCRβ-BV711 (clone H57-597; 0.3 μl); anti-FoxP3-APC (clone FJK-16S; 1 μl); anti-Eomes-AF488 (clone Dan11mag; 1 μl); anti-CD25-PE or -BV786 (clone PC61; 0.5 μl or 0.75 μl); anti-CD44-

FITC (clone IM7; 0.2 µl); anti-CD62L-APC or –BV570 (clone MEL-14; 0.2 µl or 0.25 µl, respectively); anti-CD27-PeCy7 (clone LG.7F9; 0.3 µl); anti-Tbet-PE (clone O4-46; 1 µl); from BD Bioscience (San Jose, US), ThermoFisher and BioLegend (San Diego, US). Foxp3/Transcription Factor Staining Buffer Set (eBioscience – ThermoFisher) was used for intracellular staining of FoxP3, Eomes and Tbet. Results are reported as mean fluorescence intensity (MFI) or normalized on isotype control antibody. Cells were analyzed on LSR Fortessa (BD Bioscience) and FACS data were collected with DIVA software (version 6.1.1 or 6.2). Data were analyzed with FlowJo software (version 9.9.6) (Treestar, Ashland, US).

Purification of tumor infiltrating immune cells

Cells from tumors were stained with CD45-BV605, CD11b-BV786, Ly6G-PECF594, CD11c-AF700, Ly6C-BV421, F4/80-PeCy7, CD3-PerCP, CD4-AF700 and CD8a-PE. Neutrophils ($CD45^+$, $CD11b^+$, $Ly6G^+$), monocytes ($CD45^+$, $CD11b^+$, $Ly6G^-$, $CD11c^{low}$, $F4/80^-$, $Ly6C^+$), TAMs ($CD45^+$, $CD11b^+$, $Ly6G^-$, $CD11c^{low}$, $Ly6C^-$, $F4/80^+$), $CD3^+$ ($CD45^+$, $CD11b^-$, $CD3^+$), $CD4^+$ ($CD45^+$, $CD11b^-$, $CD3^+$, $CD8^-$, $CD4^+$) and $CD8^+$ cells ($CD45^+$, $CD11b^-$, $CD3^+$, $CD8^-$, $CD4^+$) were sorted on a FACSAria cell sorter (BD Bioscience). Resulting cells were processed for mRNA extraction.

3’-mRNA sequencing

RNA was purified from FACS sorted MN/MCA1 tumor-infiltrating monocytes and TAMs deriving from wt and $C3^{-/-}$ mice (4 biological replicates each) with Single Cell RNA Purification Kit (Norgen Biotek Corp.). RNA quality control was performed with Agilent 4200 Tape Station system using High Sensitivity RNA ScreenTape analysis kit (Agilent, Santa Clara, CA, USA). Only RNAs having a RIN>7.5 were used for library preparation. Libraries were prepared starting from 5 ng totRNA for each sample by using SMART-Seq v4 Ultra Low Input RNA Kit (Clontech-Takara), based on Clontech’s proprietary SMART® (Switching Mechanism at 5’ End of RNA Template) technology. Full-length cDNAs were processed with Nextera XT DNA Library Preparation Kits (Illumina, San Diego, CA, USA). Libraries were checked using Agilent TapeStation 4200 using High Sensitivity DNA ScreenTape analysis kit. Samples were sequenced on Illumina NextSeq 500 at an average of 29,246,059 bases-long, single-end reads; among these an average of 26,000,253 reads were uniquely mapped.

Computational analyses

TCGA data of human sarcoma were derived from the cBioportal platform (http://www.cbioportal.org/). Expression data were used as available in the file “data_RNA_Seq_v2_expression_median.txt”, containing v2 processed normalized counts.

Raw reads of in-house performed RNA-Seq were quality controlled with FastQC, version 0.11.8, (https://www.bioinformatics.babraham.ac.uk/projects/fastqc/) and FastQ Screen software, version 0.13.0 (https://www.bioinformatics.babraham.ac.uk/projects/fastq_screen/) and subsequently mapped on mouse genome Release M20 (GRCm38.p6) with STAR [50], version 2.7.1a. Gene summarized quantifications were obtained by running STAR with GENCODE annotation M20.

Subsequent statistical analyses and plots based were created using the R environment, version 3.5.2. Heatmaps were generated with R package “pheatmap” version 1.0.12 (https://CRAN.R-project.org/package=pheatmap), volcano plots with R package “EnhancedVolcano” (https://github.com/kevinblighe/EnhancedVolcano), version 1.0.1, scatterplots and PCA plots with the package “ggplot2” (https://cran.r-project.org/web/packages/ggplot2/index.html), version 3.3.2.

Ensembl gene identifiers were associated to gene symbols with the R package “org.Mm.eg.db” version 3.7.0 (http://bioconductor.org/packages/release/data/annotation/html/org.Mm.eg.db.html. Star quantified read counts were normalised with rlog method into DESeq2 R package, version 1.22.2, filtering genes whose expression across samples was <2. Differential expression analyses were performed with DESeq2 [51]. Several geneset analysis algorithms were used to define pathways enrichments: preranked geneset enrichment analysis (preranked GSEA) was performed with “cameraPR.default” tool within Limma R package version 3.38.3, screening pathways derived by the Molecular Signatures Database (MSigDB) [52,53] and Gene Set Knowledgebase (GSKB), comprehensive knowledgebase for pathway analysis in mouse (GSKB: A gene set database for pathway analysis in mouse, doi: https://doi.org/10.1101/082511). gProfiler [54] and EnrichR [55,56] were used to compare enrichment results of each differential expression comparison.

Ingenuity Pathway Analysis software (QIAGEN Inc., “https://www.qiagenbioinformatics.com/products/ingenuity-pathway-analysis”) was used to identify curated sets of genes overexpressed in wt or C3-deficient cells, based on the Core Analysis function. The lists of differentially expressed genes were ranked by adjusted p-value and used to perform the analysis, a filter of 0.05 was set and mouse specific identifiers have been selected. Transcriptomic and clinical data relative to human cancer were obtained from the cBioportal platform [57], deriving normalised counts of human sarcoma of the TCGA cohort.

Custom signatures of tumor infiltrating C3-deficient macrophages and monocytes were obtained by considering human orthologues of murine genes found upregulated in C3-deficient cells (adjusted p-value <0.05 and absolute log2 fold change >1). Custom signatures representing the overall abundance of tumor infiltrating macrophages and monocytes were constituted by selecting human orthologue of differentially expressed genes in the comparison of the two cell populations.

Enrichment of defined custom signatures were attributed to each human sample in sarcoma datasets with single sample GSEA with the “GSVA” R package, version 1.30.0 [58]. An integrated score including both quantitative information and C3-deficient similarity was determined by scaling and multiplying the two values. Overall survival analyses were done by stratifying sarcoma patients based on the median value of the integrated enrichment score. The R packages “survival” (https://cran.r-project.org/web/packages/survival/index.html) version 3.2.3 and “survminer” (https://cran.r-project.org/web/packages/survminer/index.html) version 0.4.7, were used to assess statistics and draw the curves. We estimated, for each sarcoma sample within the TCGA cohort, the corresponding M1- macrophage polarization score, using CIBERSORT [29]. Subsequently, spearman

correlation was computed among the predicted enrichment of CIBERSORT-derived M1-like macrophage and the C3-deficiency scores for all sarcoma patients.

Quantitative PCR

RNA was purified using RNeasy® plus micro kit (Qiagen, Hilden, Germany). cDNA was synthesized by reverse transcription using High Capacity cDNA reverse transcriptase kit (Applied Biosystems). Pre-amplification was performed with Sso Advanced™ PreAmp Supermix (Bio-rad) according to manufacturer's instructions, using each primer at 50nM final concentration. Quantitative real-time PCR was performed using the SybrGreen PCR Master Mix (Applied Biosystems) in a QuantStudio 7Flex Real-Time PCR System (Thermo Fisher Scientific) or in a CFX96 Touch™ Real-Time PCR Detection System (Bio-Rad). PCR reactions were carried out with 10 ng of DNA. Data were analysed with the $2^{-\Delta CT}$ method. Data were normalized based on GAPDH and β-actin expression determined in the same sample. Primers were designed according to the published sequences and listed in Supplementary Table 11.

Cytokine measurement

Tumor samples were homogenized in 50mM Tris-HCl pH 7.5 containing 2mM EDTA, 1% Triton X-100, 1mM PMSF (all from Sigma-Aldrich) and protease inhibitors EDTA-Free (Complete® -EDTA-free, Roche) (1 g tumor tissue/ml). Tissue homogenates were centrifuged at 4.000 rpm, 1h at +4°C and the interphases were used to measure C5a and IFNγ with DuoSet ELISA kits (R&D systems) or C3a by ELISA (Cloud-Clone Corp.). Total proteins were measured by Pierce™ Coomassie Plus Assay Kit (Thermo Fisher) or Bio-Rad DC Protein assay kit (Bio-Rad).

Cell culture and C3 deposition assay

MN/MCA1, FS6 and 3-MCA-derived sarcoma were cultured in RPMI 1640 (Euroclone) supplemented with 10% FBS and 2 mM L-glutamine. Mouse blood was collected from the cava vein and kept on ice for 3–4 h. After centrifugation at 12.000 rcf for 12 min at +4°C, serum was collected and stored at −80°C. Complement inactivation was obtained by worming serum at +56°C for 30 min. For deposition assay, sarcoma cells or cells obtained by peritoneal washes of wt mice were incubated for 5 min at +37°C with Veronal Buffer 1X (Lonza) containing 10% of normal or heat inactivated (HI) serum. Then, complement activation was immediately blocked by keeping the cells on ice and by adding EDTA at 10 mM final concentration. Cells were washed, fixed for 10 min with PFA 1% at RT and used for the staining. Briefly, samples were blocked in PBS^{++} containing 2% BSA and 5% Normal Donkey Serum (NDS, Sigma) for 30 min at RT and then stained for 1h at RT with 5μg/ml anti-mouse C3b/iC3b/C3c (Hycult Biotech, clone 2/11) primary antibody or relative isotype control (rat IgG1λ, BD Pharmingen™). Cells were fixed with PFA 1% for 5 min, washed and incubated with 2 μg/ml AF488-donkey anti-rat IgG secondary antibody (Molecular Probes - ThermoFisher), for 1h at RT. Cells were analysed on Canto II (BD Bioscience) and data were analysed with FlowJo software (Treestar). In selected experiments, sarcoma cells were pre-incubated overnight at 37°C with 10μg/ml tunicamycin (Sigma-Aldrich), or vehicle (0.1% DMSO), in complete medium and then subjected to C3 deposition assay. Staining for terminal residues of galactose, mannose, α-(2➔3) and

α-(2➔6) sialic acid was performed after cell fixation with PFA 1% for 10 min at RT, by incubating samples for 1h at RT with 2 μg/ml of digoxigenin-conjugated lectins DSA, GNA, MAA and SNA (from DIG Glycan Differentiation Kit, Roche™). Then, samples were incubated with FITC-anti-digoxigenin antibody (Abcam, clone 21H8), 2 μg/ml, and analysed by FACS.

Immunofluorescence

MN/MCA1 cells and wt peritoneal macrophages were cultured for 1h at +37°C on cover glasses (VWR international) pre-coated with 0.001% of poly-lysine (Sigma-Aldrich) and fixed with PFA 1% for 15 min at RT. MN/MCA1- or 3-MCA-derived tumors were fixed with PFA 4% overnight at +4°C and embedded in OCT after a graded sucrose series. Fixed cells and tumor sections (7μm) were incubated for 1 or 2h, respectively, at RT with primary antibodies diluted in PBS^{++} pH 7.4 containing 2% BSA (Sigma-Aldrich), 5% normal donkey (Sigma-Aldrich) or goat (Dako, Denmark) serum (according to secondary antibody source) and 0.05% Triton X-100 (Sigma-Aldrich) (blocking solution). The following primary antibodies and final concentrations were used: anti-mouse C3aR (Hycult Biotech, clone 14D4, 1 μg/ml), anti-mouse C3b/iC3b/C3c (Hycult Biotech, clone 2/11, 5 μg/ml), anti-CD31 (Millipore, clone 2H8, 1 μg/ml), anti-CD45 (Abcam, rabbit polyclonal, 5 μg/ml), anti-Iba-1 (FUJIFILM Wako Pure Chemical Corporation, rabbit polyclonal, 2 μg/ml), and anti-NG2 (Millipore, rabbit polyclonal, 5 μg/ml). Negative controls were obtained by using isotype matched antibodies. Samples were then incubated with Alexa Fluor (488, 594, 647)-conjugated species-specific cross-adsorbed detection antibodies (Molecular Probes) for 1 or 2h at RT. For DNA detection, 4',6-diamidino-2-phenylindole (DAPI) (300nM, Invitrogen) was used. Samples were mounted with the antifade medium FluorPreserve Reagent (EMD Millipore) and analysed with a Leica SP8 confocal microscope system equipped with Leica HC PL APO 20x/0.4 NA objective at 1 AU. Alexa Fluor-488, −594 and −647 were excited with a 488, 552 and 638nm diode Laser and emission collected from 505 to 550, 580 to 620 and 650 to 750 nm, respectively. Collected *xy* images were assembled and processed using LASX software. Density of CD31-positive blood vessels and vessel pericyte coverage were calculated as described [59].

Immunohistochemistry on human samples

Tumor paraffin embedded tissues were cut at 3-μm and sections were dewaxed with Xilol and rehydrated with decreasing concentrations of Ethanol to water. Antigen unmasking was performed in 0.25mM EDTA buffer pH 8.00 in thermostatic bath at 98°C for 20 min (C1q and C3aR staining), in 0.25mM EDTA buffer pH 8.00 in decloaking chamber (125°C for 3 min and then 90°C for 5 min) (C4d staining) or not performed (C3c staining). Endogenous peroxidase was blocked using 3% hydrogen peroxide solution for 20 min at RT. Sections were then blocked with 2% BSA in PBS for 30 min and incubated with the following antibodies and final concentration: rabbit polyclonal anti human-C1q (Dako Cytomation, 14.2 μg/ml), rabbit polyclonal anti-human C3c antibody (Dako Cytomation, 6.4 μg/ml), mouse monoclonal anti-human C4d antibody (clone LP69, Abcam, 34 μg/ml), mouse monoclonal anti-human C3aR antibody (clone 17, Santa Cruz Biotechnology, 1 μg/ml) for 30 min (C3c staining) or 1h (C1q, C4d and C3aR staining) at RT. Sections were then incubated with MACH1 Universal HRP Polymer Kit at RT (Biocare Medical). After

a 3,3′-Diaminobenzidine (DAB) reaction (Biocare Medical), sections were counterstained with haematoxylin, dehydrated with ethanol and mounted with Eukitt (Sigma-Aldrich). Ten images for each sample (magnification 20X) were acquired with cell^F software (Olympus) on Olympus BX51 microscope and analyzed with Image Pro-Premiere 9.2 (Media Cybernetics). The IRA percentage for C3aR in the tumors was determined and was employed to divide patients showing negative or positive staining for C3aR expression. Patients (n=19) gave their signed consent to donate the tissue remaining after diagnostic procedures. UPS surgical samples were collected from the Center for Biological Resources of Humanitas Clinical and Research Center. The study was approved by Humanitas Clinical and Research Center Ethical Committee (authorization 609/17, issued on 18/12/2017).

Statistics and Reproducibility

For animal studies, sample size was defined on the basis of past experience on cancer models, to detect differences of 20% or greater between the groups (10% significance level and 80% power).

In most in vivo experiments the investigators were unaware of the genotype of the experimental groups or of the treatment performed. In other in vivo studies, blinding was not possible because only one operator performed both the initial carcinogen/tumor cell injection and the following tumor volume measurements. The operator was unaware of mouse genotype or patients' clinical data during the acquisition of fields and quantification of IF on mouse samples and IHC of human samples. For in vitro experiments (e.g. FACS, RT-PCR, IF, ELISA, RNAseq), blinding was not considered relevant because the analysis was not operator-dependent. Values were expressed as mean ± SE. Two-tailed Wilcoxon matched-pairs signed-rank test was used to compare two groups for tumor incidence. Two-tailed Student's t test and Mann–Whitney U-test were used to compare unmatched groups with Gaussian and non-Gaussian distribution, respectively, and Welch's correction was applied in cases of significantly different variance. A ROUT test was applied to exclude outliers. Ordinary one-way ANOVA and Kruskal Wallis were used to compare multiple groups with Gaussian and non-Gaussian distribution, respectively, and unpaired Student's t test or Mann–Whitney U-test were used as *post hoc* tests. The Kaplan-Meier method was used for survival curve analysis, and the log-rank (Mantel-Cox) test was used to determine the statistical significance. $p \leq 0.05$ was considered significant. Statistics were calculated with GraphPad Prism version 7, GraphPad software.

Data availability.—All data are present in the main text and/or in supplementary information. RNA sequencing datasets are available in the NCBI Gene Expression Omnibus (GEO) under accession number GSE141692. Data relative to human sarcoma were downloaded as available on the cBioportal platform (http://www.cbioportal.org/study/summary?id=sarc_tcga). Further information on research design is available in the Nature Research Reporting Summary linked to this article. Source data are available for this study. All other data supporting the findings of this study are available from the corresponding author on reasonable request.

Code availability: All custom scripts developed to perform the analyses are available at https://figshare.com/articles/software/Custom_R_scripts_related_to_fig5_fig7_and_suppl_fig5/13286225

Extended Data

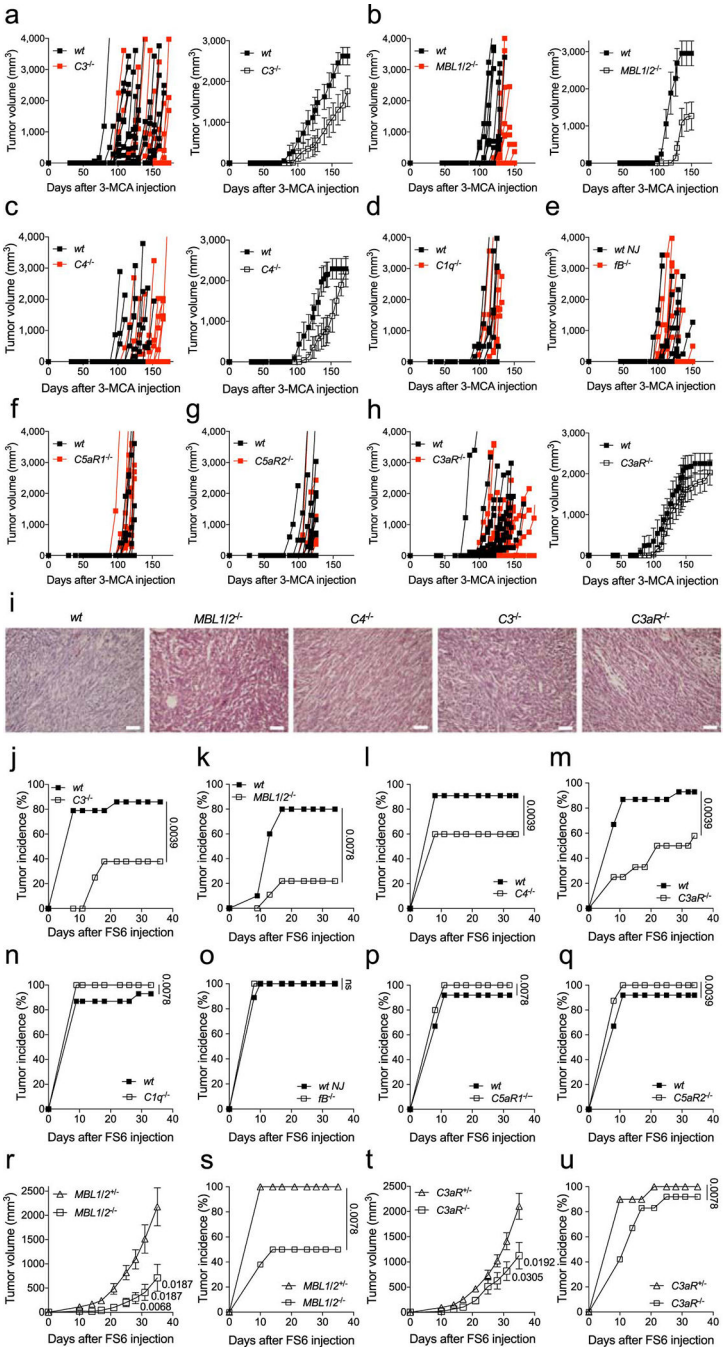

Extended Data Fig. 1: The lectin pathway and the C3aR promote 3-MCA-induced sarcomagenesis and FS6 sarcoma growth.

(a-h) 3-MCA-induced sarcoma growth curves (left panels) or mean tumor volume (± SEM, right panels) in *C3*$^{-/-}$ (a, n=20 wt, n=18 ko), *MBL1/2*$^{-/-}$ (b, n=10 wt, n=14 ko), *C4*$^{-/-}$ (c, n=10 mice in each group), *C1q*$^{-/-}$ (d, n=7 wt, n=8 ko), *fB*$^{-/-}$ (e, n=9 wt, n=12 ko), *C5aR1*$^{-/-}$ (f, n=10 wt, n=19 ko), *C5aR2*$^{-/-}$ (g, n=14 wt, n=10 ko) and *C3aR*$^{-/-}$ (h, n=14 wt, n=16 ko) mice. Experiment of panel d was performed using wt littermates. (i) Representative H&E staining of 3-MCA tumor tissues of wt, *C3*$^{-/-}$, *MBL1/2*$^{-/-}$, *C4*$^{-/-}$ and *C3aR*$^{-/-}$ mice. One experiment performed, three representative fields have been acquired for each group (n=4 mice in each group). Scale bar: 100μm. (j-q) FS6 tumor incidences in *C3*$^{-/-}$ (j, n= 4 wt, n=8 ko); *MBL1/2*$^{-/-}$ (k, n=10 wt, n=9 ko); *C4*$^{-/}$ (l, n=11 wt, n=10 ko); *C3aR*$^{-/-}$ (m, n=15 wt, n=12 ko); *C1q*$^{-/-}$ (n, n=15 wt, n=8 ko); *fB*$^{-/-}$ (o, n=9 wt, n=4 ko); *C5aR1*$^{-/-}$ (p, n=12 wt, n=5 ko) and *C5aR2*$^{-/-}$ (q, n=12 wt, n=8 ko) mice. (r-u) FS6 tumor volumes (mean ± SEM) (r, t) and incidences (s, u) in *MBL1/2*$^{\pm/-}$ (r-s, n=12 he, n=8 ko) and *C3aR*$^{\pm/-}$ (t-u, n=21 he, n=12 ko) littermates. One representative experiment out of three (a), two (b, d, e, f, j and k) or one (c, g, h, l, n, p, q, r, s, t and u) performed is shown. o, m: two pooled experiments. The same wt mice were used simultaneously as control mice of experiments of panels p, q and one out of the two pooled experiments of panel m. Two-tailed Mann Whitney test (r) or unpaired two-tailed Student's t test (t). Exact p values are reported, two-tailed Wilcoxon matched-pairs signed rank test (j-q, s and u).

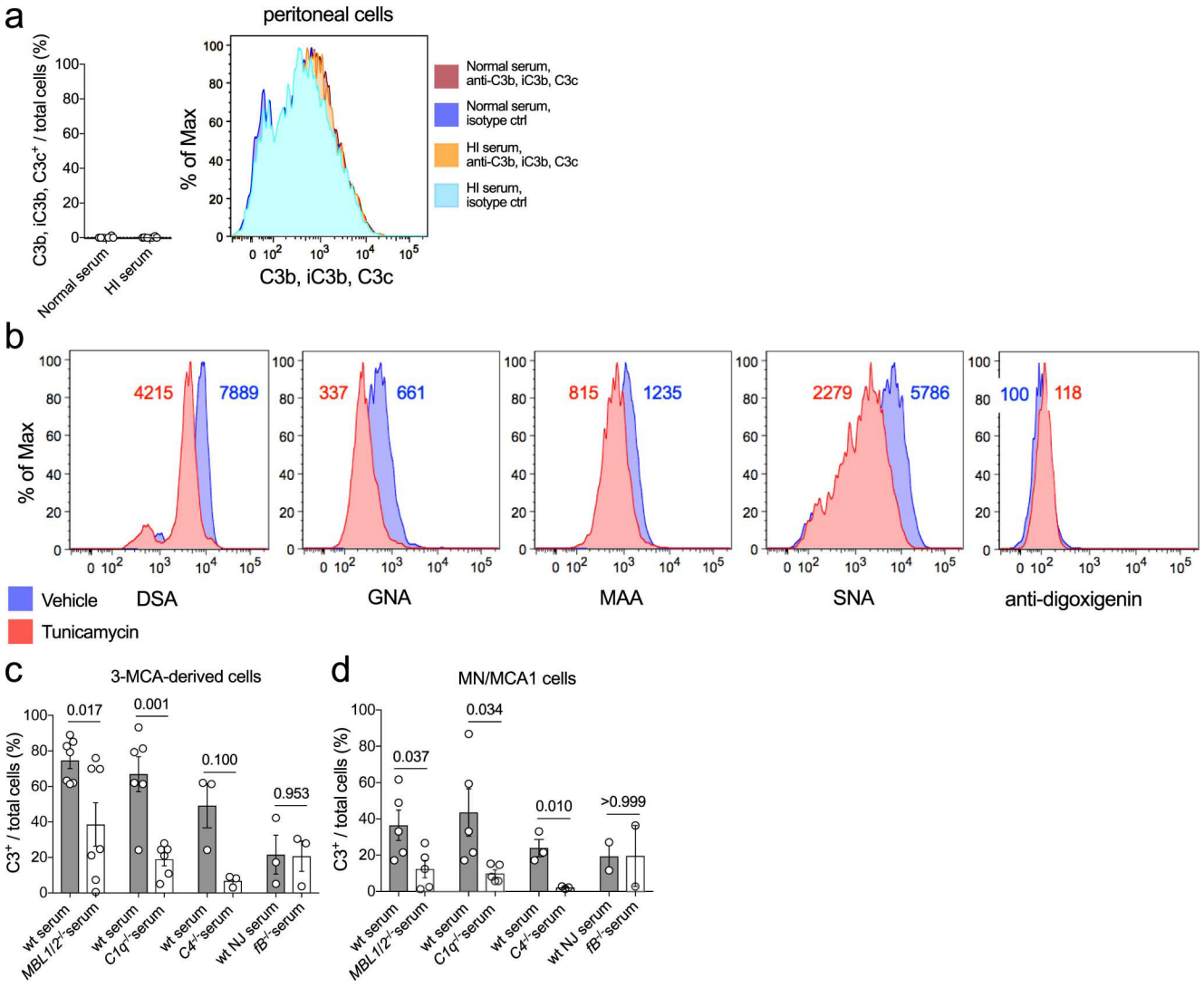

Extended Data Fig. 2: Complement deposition on sarcoma cells.

(a) Flow cytometry analysis of C3b, iC3b, C3c deposition on cells derived from peritoneal washes of wt mice incubated with heat inactivated (HI) or normal serum. Representative FACS plot from a single mouse (right panel) and quantification of C3b, iC3b, C3c-positive cells on total cells is shown (left panel) (n=6 different mice, mean ± SEM). (b) Representative FACS plots showing the staining with digoxigenin-labeled DSA, GNA, MAA and SNA lectins or anti-digoxigenin alone in 3-MCA-derived sarcoma cells treated with 10μg/ml tunicamycin (red) or vehicle (blu). (c-d) Flow cytometry analysis of C3b, iC3b, C3c deposition on 3-MCA-derived (c) and MN/MCA1 (d) sarcoma cells incubated with normal serum from wt and *MBL1/2*$^{-/-}$ [n=7 (c) and n=5 (d) independent experiments], *C1q*$^{-/-}$ [n=6 (c) and n=5 (d) independent experiments], *C4*$^{-/-}$ [n=3 (c and d) independent experiments] or *fB*$^{-/-}$ [n=3 (c) and n=2 (d) independent experiments] (mean ± SEM). For some experiments the same normal wt serum was used as control of different ko sera. Exact p values are reported. Two-tailed Mann Whitney test (c, *C4*$^{-/-}$ serum) or unpaired two-tailed Student's t test (c, excluding *C4*$^{-/-}$ serum, and d).

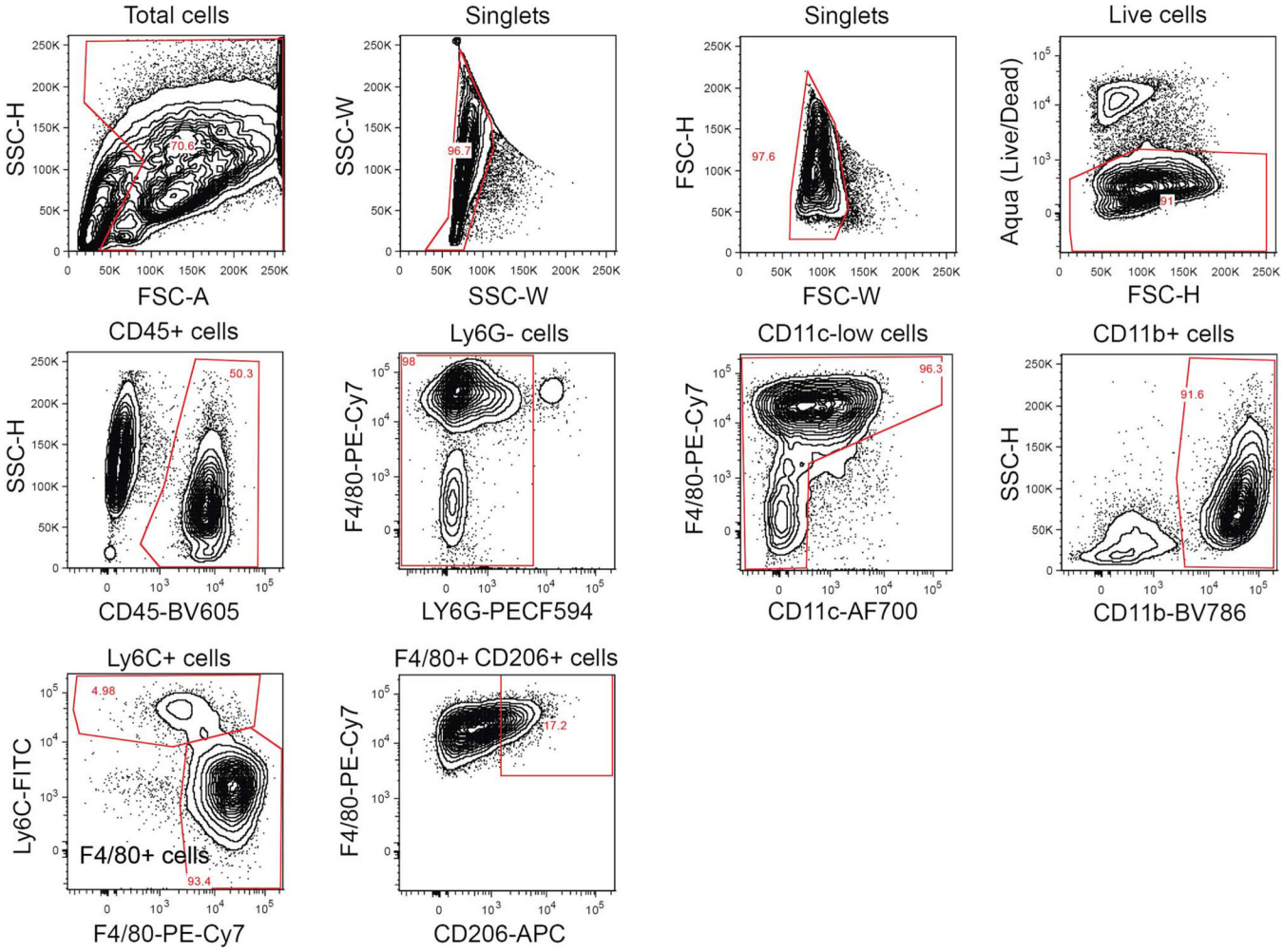

Extended Data Fig. 3: Gating strategy for FACS analysis of TAMs and monocytes in MN/MCA1 sarcomas.

Representative FACS plots showing the gating strategy for FACS analysis of TAMs and monocytes in MN/MCA1 tumor samples. Gate of F4/80+ cells corresponds to FACS data panels of F4/80$^+$/Aqua$^-$ (%) of Figures 4d, 4j and Extended Data Figure 4b. Gate of F4/80$^+$ CD206$^+$ cells corresponds to FACS data panels of F4/80$^+$ CD206$^+$/Aqua$^-$ (%) of Figures 4f, 4h, 4k and Extended Data Figure 4b. The expression of selected M1 markers (CD11c, MHC II, CD80 and CD86), reported as MFI in FACS data panels of Figures 4g, 4i, 4l and Extended Data Figure 4a–b, is gated on F4/80$^+$ cells. Gate of Ly6C$^+$ cells corresponds to FACS data panels of Ly6C$^+$/Aqua$^-$ (%) of Figures 4e, 4j and Extended Data Figure 4a–b.

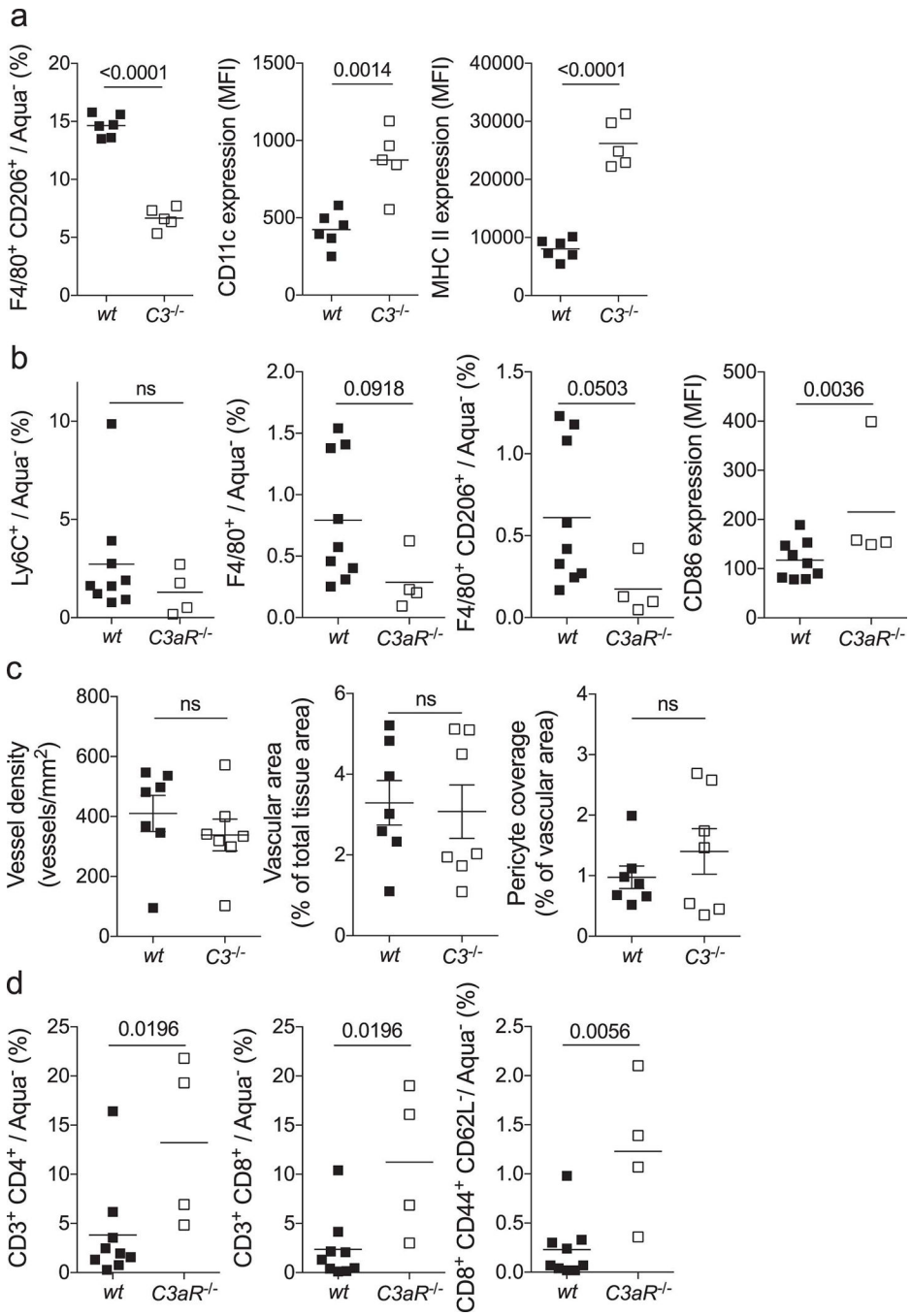

Extended Data Fig. 4: Effect of C3 and C3aR deficiency on TAMs and T cells in im injected MN/MCA1 and FS6 models.

(a) Analysis by FACS of M2 macrophage frequency ($F4/80^+CD206^+$) and of selected M1 marker (CD11c, MHC II, measured as MFI) expression gated on total macrophages ($F4/80^+$) in wt and $C3^{-/-}$ mice sacrificed 27 days after im MN/MCA1 tumor cell injection (n=6 wt mice, n=5 ko mice, mean ± SEM). (b) Analysis by FACS of monocyte ($Ly6C^+$), macrophage ($F4/80^+$), M2 macrophage frequency ($F4/80^+CD206^+$) and of CD86 (measured as MFI) expression gated on total macrophages ($F4/80^+$) in wt and $C3aR^{-/-}$ mice sacrificed 34 days after FS6 tumor cell injection (n=9 wt mice, n=4 ko mice; mean ± SEM). (c) Quantitation of

vessel density, vascular area and vascular coverage by pericytes in 3-MCA-derived tumors of wt and *C3*$^{-/-}$ mice (n=7 mice in each group; mean ± SEM). (d) Frequency of $CD3^+CD4^+$, $CD3^+CD8^+$ and activated effector/effector memory T cells ($CD8^+CD44^+CD62L^-$) in wt and *C3aR*$^{-/-}$ mice sacrificed 34 days after FS6 tumor cell injection (n=9 wt mice, n=4 ko mice; mean ± SEM). a-d: one experiment performed. Exact p values are reported, unpaired two-tailed Student's t test or two-tailed Mann Whitney test (a-d).

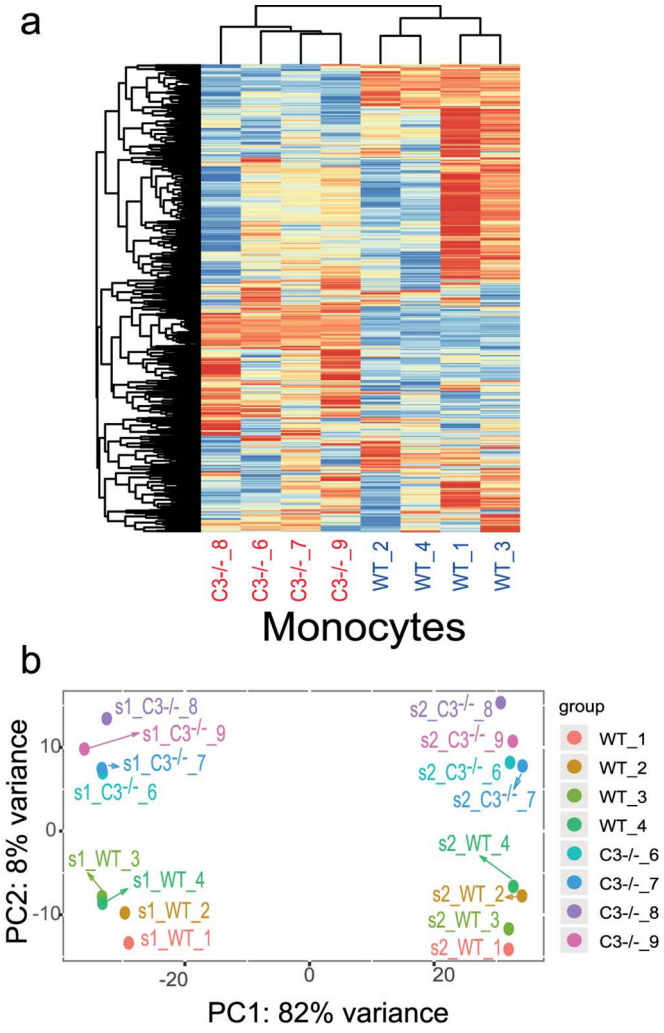

c

Cell population	DE genes Down in KO	DE genes UP in KO	Human orthologue Down in KO	Human orthologue Up in KO
Macrophages	177	120	135	60
Monocytes	145	152	115	85

Extended Data Fig. 5: Transcriptional profiling analysis of sarcoma infiltrating monocytes.

(a) Heatmap showing the first 1000 more differentially expressed genes in wt (blue) versus C3-deficient (red) monocytes. (b) PC analysis of RNA expression of macrophages and monocytes. X and Y axes represent the first and the second PC, respectively. (c) Number of differentially expressed mouse genes and human orthologues in tumor infiltrating leukocytes.

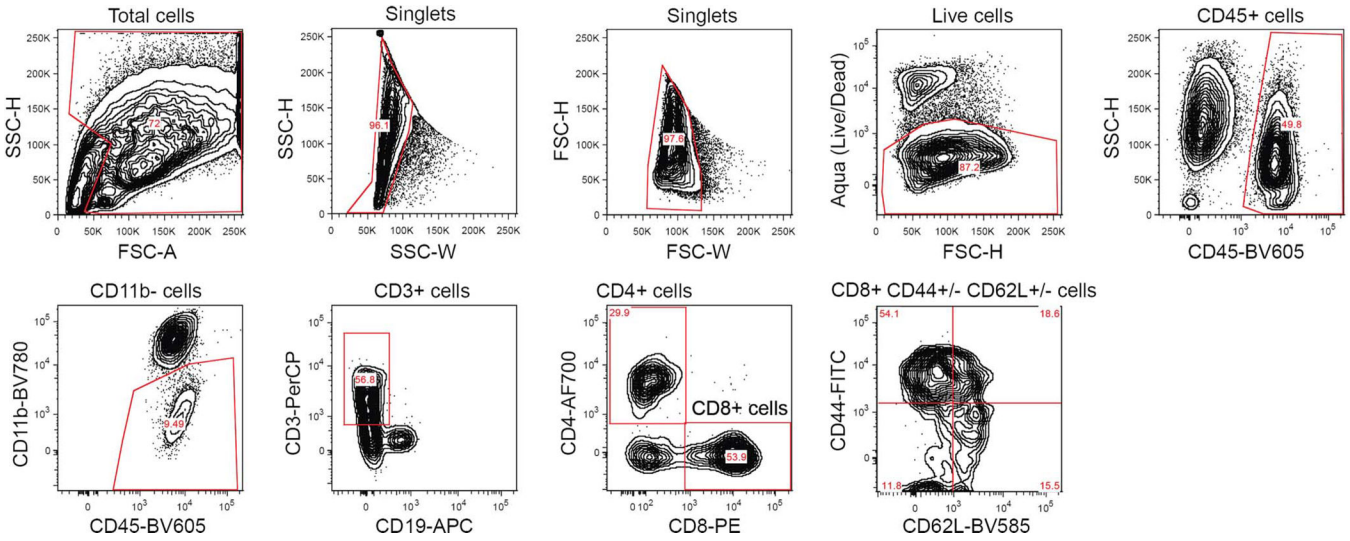

Extended Data Fig. 6: Gating strategy for FACS analysis of CD4$^+$, CD8$^+$ and CD44$^+$CD62L$^-$CD8$^+$ T cells in MN/MCA1 sarcomas.

Representative FACS plots showing the gating strategy for FACS analysis of CD4$^+$, CD8$^+$ and CD44$^+$ CD62L$^-$ CD8$^+$ T cells in MN/MCA1 tumor samples. Gate of CD4$^+$ cells corresponds to FACS data panels of CD4$^+$/Aqua$^-$ (%) of Figures 6a, 6g and Extended Data Figure 4d. Gate of CD8$^+$ cells corresponds to FACS data panels of CD8$^+$/Aqua$^-$ (%) of Figures 6e, 6g and Extended Data Figure 4d. Gate of CD44$^+$CD62L$^-$CD8+ cells (upper right panel) corresponds to FACS data panels of CD8$^+$ CD44$^+$ CD62L$^-$/Aqua$^-$ (%) of Figures 6f, 6g and Extended Data Figure 4d.

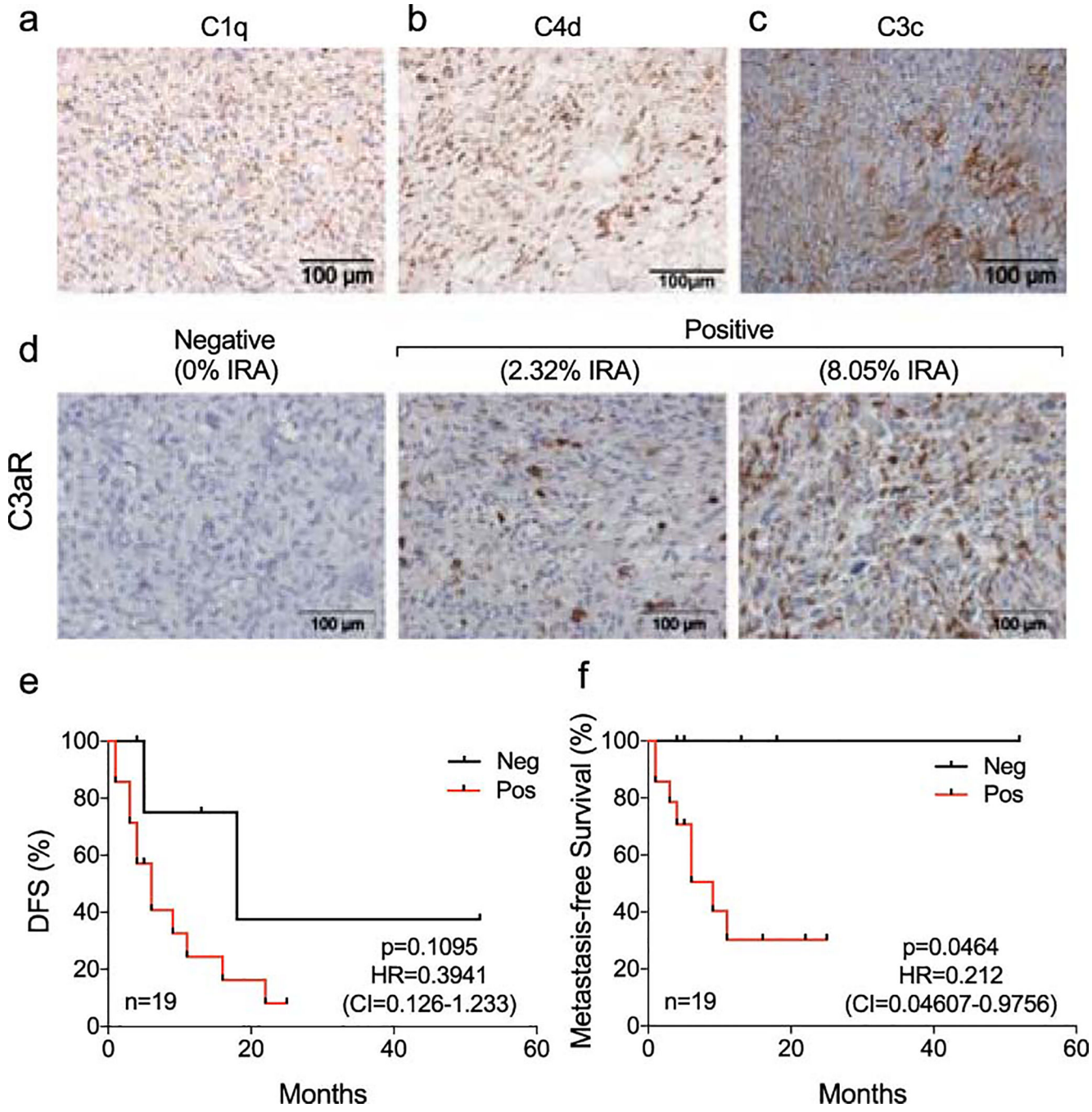

Extended Data Fig. 7: Complement activation and prognostic significance of C3aR expression in UPS patients.

(a-d) Representative magnification images (20X) of immunostaining analysis for C1q (a), C4d (b), C3c (c) and C3aR (d) in UPS tissue sections. One experiment performed (n=19 patients), 10 representative fields have been acquired for each patient. Representative images for patients showing negative (0% IRA, left panel) or positive (>0% IRA, central and right panels) staining for C3aR expression (d). Scale bar: 100µm. (e-f) Kaplan-Meier survival curves representing the DFS (e) and the metastasis-free survival (f) for patients showing negative (n=5 patients) or positive (n=14 patients) staining for C3aR expression. Exact p

value of Log-rank test for survival curves, Hazard ratio (HR) and confidence intervals (CI) are indicated in the figures (e, f).

Supplementary Material

Refer to Web version on PubMed Central for supplementary material.

Acknowledgments

We thank F.S. Colombo for cell sorting experiments, J. Cibella for technical help in RNAseq experiments and F. Grizzi for technical help in IHC experiments. The contributions of Fondazione Cariplo (Contract no. 2016–0568 to E.M.); Ministero della Salute (RF-2013–02355470 to C.G.); the European Commission (ERC project PHII-669415), Ministero dell'Istruzione, dell'Università e della Ricerca (MIUR) (PRIN 2015YYKPNN and 20174T7NXL), and Associazione Italiana Ricerca sul Cancro (AIRC IG-19014 to A.M. and AIRC IG-21714 to C.G.), and National Institute of Health (AI068730 to J.D.L) are gratefully acknowledged. E.M. has been recipient of a fellowship from Fondazione Umberto Veronesi (FUV, 2016–2017). We acknowledge CINECA and ELIXIR, for the availability of high performance computing resources and support.

References

1. Balkwill F & Mantovani A Inflammation and cancer: back to Virchow? Lancet 357, 539–545 (2001). [PubMed: 11229684]
2. Mantovani A, Allavena P, Sica A & Balkwill F Cancer-related inflammation. Nature 454, 436–444 (2008). [PubMed: 18650914]
3. Coussens LM, Zitvogel L & Palucka AK Neutralizing tumor-promoting chronic inflammation: a magic bullet? Science 339, 286–291 (2013). [PubMed: 23329041]
4. Qian BZ & Pollard JW Macrophage diversity enhances tumor progression and metastasis. Cell 141, 39–51 (2010). [PubMed: 20371344]
5. Mantovani A, Marchesi F, Malesci A, Laghi L & Allavena P Tumour-associated macrophages as treatment targets in oncology. Nat Rev Clin Oncol 14, 399–416 (2017). [PubMed: 28117416]
6. Mantovani A & Allavena P The interaction of anticancer therapies with tumor-associated macrophages. J Exp Med 212, 435–445 (2015). [PubMed: 25753580]
7. Bottazzi B, Doni A, Garlanda C & Mantovani A An integrated view of humoral innate immunity: pentraxins as a paradigm. Annu Rev Immunol 28, 157–183 (2010). [PubMed: 19968561]
8. Reis ES, Mastellos DC, Ricklin D, Mantovani A & Lambris JD Complement in cancer: untangling an intricate relationship. Nat Rev Immunol 18, 5–18 (2018). [PubMed: 28920587]
9. Roumenina LT, Daugan MV, Petitprez F, Sautes-Fridman C & Fridman WH Context-dependent roles of complement in cancer. Nat Rev Cancer 19, 698–715 (2019). [PubMed: 31666715]
10. Golay Jet al.CD20 levels determine the in vitro susceptibility to rituximab and complement of B-cell chronic lymphocytic leukemia: further regulation by CD55 and CD59. Blood98, 3383–3389 (2001). [PubMed: 11719378]
11. Fishelson Z & Kirschfink M Complement C5b-9 and Cancer: Mechanisms of Cell Damage, Cancer Counteractions, and Approaches for Intervention. Front Immunol 10, 752 (2019). [PubMed: 31024572]
12. Surace Let al.Complement is a central mediator of radiotherapy-induced tumor-specific immunity and clinical response. Immunity42, 767–777 (2015). [PubMed: 25888260]
13. West EE, Kolev M & Kemper C Complement and the Regulation of T Cell Responses. Annu Rev Immunol 36, 309–338 (2018). [PubMed: 29677470]
14. Ning Cet al.Complement activation promotes colitis-associated carcinogenesis through activating intestinal IL-1beta/IL-17A axis. Mucosal Immunol8, 1275–1284 (2015). [PubMed: 25736459]
15. Ajona D, Ortiz-Espinosa S & Pio R Complement anaphylatoxins C3a and C5a: Emerging roles in cancer progression and treatment. Semin Cell Dev Biol 85, 153–163 (2019). [PubMed: 29155219]
16. Afshar-Kharghan VThe role of the complement system in cancer. J Clin Invest127, 780–789 (2017). [PubMed: 28248200]

17. Markiewski MMet al.Modulation of the antitumor immune response by complement. Nat Immunol9, 1225–1235 (2008). [PubMed: 18820683]
18. Vadrevu SKet al.Complement c5a receptor facilitates cancer metastasis by altering T-cell responses in the metastatic niche. Cancer Res74, 3454–3465 (2014). [PubMed: 24786787]
19. Cao Q, McIsaac SM & Stadnyk AW Human colonic epithelial cells detect and respond to C5a via apically expressed C5aR through the ERK pathway. Am J Physiol Cell Physiol 302, C1731–1740 (2012). [PubMed: 22496247]
20. Roumenina LTet al.Tumor Cells Hijack Macrophage-Produced Complement C1q to Promote Tumor Growth. Cancer Immunol Res7, 1091–1105 (2019). [PubMed: 31164356]
21. Bonavita Eet al.PTX3 is an extrinsic oncosuppressor regulating complement-dependent inflammation in cancer. Cell160, 700–714 (2015). [PubMed: 25679762]
22. Rubino Met al.Epigenetic regulation of the extrinsic oncosuppressor PTX3 gene in inflammation and cancer. Oncoimmunology6, e1333215 (2017). [PubMed: 28811977]
23. Hajishengallis G, Reis ES, Mastellos DC, Ricklin D & Lambris JD Novel mechanisms and functions of complement. Nat Immunol 18, 1288–1298 (2017). [PubMed: 29144501]
24. Ponzetta Aet al.Neutrophils Driving Unconventional T Cells Mediate Resistance against Murine Sarcomas and Selected Human Tumors. Cell178, 346–360 e324 (2019). [PubMed: 31257026]
25. Katenkamp D, Kosmehl H & Langbein L In adequate tumor surgery of chemically induced soft tissue sarcomas--an experimental approach for induction of metastasis formation? Exp Pathol 34, 209–215 (1988). [PubMed: 3234510]
26. Li Qet al.Transformation potential of bone marrow stromal cells into undifferentiated high-grade pleomorphic sarcoma. J Cancer Res Clin Oncol136, 829–838 (2010). [PubMed: 19936790]
27. Molgora Met al.IL-1R8 is a checkpoint in NK cells regulating anti-tumour and anti-viral activity. Nature551, 110–114 (2017). [PubMed: 29072292]
28. Taylor BSet al.Advances in sarcoma genomics and new therapeutic targets. Nat Rev Cancer11, 541–557 (2011). [PubMed: 21753790]
29. Newman AMet al.Robust enumeration of cell subsets from tissue expression profiles. Nat Methods12, 453–457 (2015). [PubMed: 25822800]
30. Cho MSet al.Autocrine effects of tumor-derived complement. Cell Rep6, 1085–1095 (2014). [PubMed: 24613353]
31. Nunez-Cruz Set al.Genetic and pharmacologic inhibition of complement impairs endothelial cell function and ablates ovarian cancer neovascularization. Neoplasia14, 994–1004 (2012). [PubMed: 23226093]
32. Guglietta Set al.Coagulation induced by C3aR-dependent NETosis drives protumorigenic neutrophils during small intestinal tumorigenesis. Nat Commun7, 11037 (2016). [PubMed: 26996437]
33. Nabizadeh JAet al.The Complement C3a Receptor Contributes to Melanoma Tumorigenesis by Inhibiting Neutrophil and CD4+ T Cell Responses. J Immunol196, 4783–4792 (2016). [PubMed: 27183625]
34. Doerner SKet al.High-Fat Diet-Induced Complement Activation Mediates Intestinal Inflammation and Neoplasia, Independent of Obesity. Mol Cancer Res14, 953–965 (2016). [PubMed: 27535705]
35. Wang Yet al.Autocrine Complement Inhibits IL10-Dependent T-cell-Mediated Antitumor Immunity to Promote Tumor Progression. Cancer Discov6, 1022–1035 (2016). [PubMed: 27297552]
36. Boire Aet al.Complement Component 3 Adapts the Cerebrospinal Fluid for Leptomeningeal Metastasis. Cell168, 1101–1113 e1113 (2017). [PubMed: 28283064]
37. Ajona Det al.A Combined PD-1/C5a Blockade Synergistically Protects against Lung Cancer Growth and Metastasis. Cancer Discov7, 694–703 (2017). [PubMed: 28288993]
38. de Visser KE, Korets LV & Coussens LM Early neoplastic progression is complement independent. Neoplasia 6, 768–776 (2004). [PubMed: 15720803]
39. Medler TRet al.Complement C5a Fosters Squamous Carcinogenesis and Limits T Cell Response to Chemotherapy. Cancer Cell34, 561–578 e566 (2018). [PubMed: 30300579]

40. Riihila Pet al.Complement Component C3 and Complement Factor B Promote Growth of Cutaneous Squamous Cell Carcinoma. Am J Pathol187, 1186–1197 (2017). [PubMed: 28322200]
41. Aykut Bet al.The fungal mycobiome promotes pancreatic oncogenesis via activation of MBL. Nature574, 264–267 (2019). [PubMed: 31578522]
42. Hanahan D & Weinberg RA Hallmarks of cancer: the next generation. Cell 144, 646–674 (2011). [PubMed: 21376230]
43. Piao Cet al.Complement 5a Enhances Hepatic Metastases of Colon Cancer via Monocyte Chemoattractant Protein-1-mediated Inflammatory Cell Infiltration. J Biol Chem290, 10667–10676 (2015). [PubMed: 25739439]
44. Czermak BJet al.In vitro and in vivo dependency of chemokine generation on C5a and TNF-alpha. J Immunol162, 2321–2325 (1999). [PubMed: 9973510]
45. Venkatesha RT, Berla Thangam E, Zaidi AK & Ali H Distinct regulation of C3a-induced MCP-1/CCL2 and RANTES/CCL5 production in human mast cells by extracellular signal regulated kinase and PI3 kinase. Mol Immunol 42, 581–587 (2005). [PubMed: 15607817]
46. Roca Het al.CCL2 and interleukin-6 promote survival of human CD11b+ peripheral blood mononuclear cells and induce M2-type macrophage polarization. J Biol Chem284, 34342–34354 (2009). [PubMed: 19833726]
47. Sica A & Mantovani A Macrophage plasticity and polarization: in vivo veritas. J Clin Invest 122, 787–795 (2012). [PubMed: 22378047]
48. Cho MSet al.Complement Component 3 Is Regulated by TWIST1 and Mediates Epithelial-Mesenchymal Transition. J Immunol196, 1412–1418 (2016). [PubMed: 26718342]
49. Petitprez Fet al.B cells are associated with survival and immunotherapy response in sarcoma. Nature577, 556–560 (2020). [PubMed: 31942077]
50. Dobin Aet al.STAR: ultrafast universal RNA-seq aligner. Bioinformatics29, 15–21 (2013). [PubMed: 23104886]
51. Love MI, Huber W & Anders S Moderated estimation of fold change and dispersion for RNA-seq data with DESeq2. Genome Biol 15, 550 (2014). [PubMed: 25516281]
52. Subramanian Aet al.Gene set enrichment analysis: a knowledge-based approach for interpreting genome-wide expression profiles. Proc Natl Acad Sci U S A102, 15545–15550 (2005). [PubMed: 16199517]
53. Liberzon Aet al.Molecular signatures database (MSigDB) 3.0. Bioinformatics27, 1739–1740 (2011). [PubMed: 21546393]
54. Raudvere Uet al.g:Profiler: a web server for functional enrichment analysis and conversions of gene lists (2019 update). Nucleic Acids Res47, W191–W198 (2019). [PubMed: 31066453]
55. Kuleshov MVet al.Enrichr: a comprehensive gene set enrichment analysis web server 2016 update. Nucleic Acids Res44, W90–97 (2016). [PubMed: 27141961]
56. Chen EYet al.Enrichr: interactive and collaborative HTML5 gene list enrichment analysis tool. BMC Bioinformatics14, 128 (2013). [PubMed: 23586463]
57. Cerami Eet al.The cBio cancer genomics portal: an open platform for exploring multidimensional cancer genomics data. Cancer Discov2, 401–404 (2012). [PubMed: 22588877]
58. Hanzelmann S, Castelo R & Guinney J GSVA: gene set variation analysis for microarray and RNA-seq data. BMC Bioinformatics 14, 7 (2013). [PubMed: 23323831]
59. Magrini Eet al.Endothelial deficiency of L1 reduces tumor angiogenesis and promotes vessel normalization. J Clin Invest124, 4335–4350 (2014). [PubMed: 25157817]

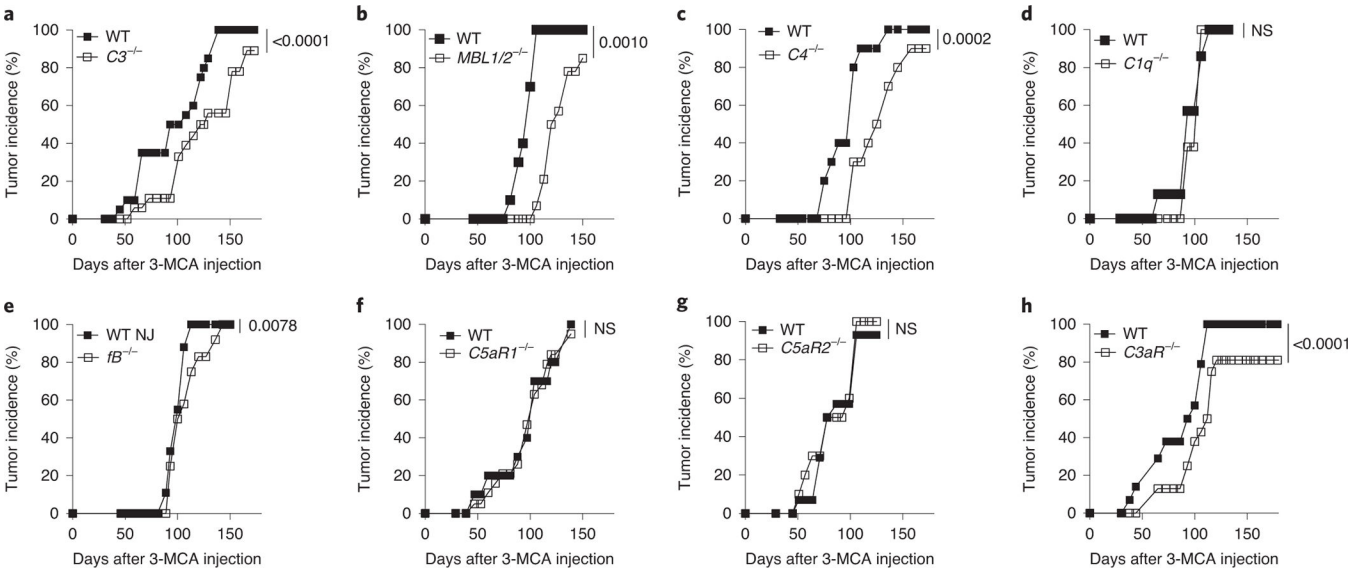

Figure 1. The lectin pathway and the C3aR promote 3-MCA-induced sarcomagenesis

(a-h) 3-MCA-induced sarcoma incidence in $C3^{-/-}$ (a, n=20 wt, n=18 ko), $MBL1/2^{-/-}$ (b, n=10 wt, n=14 ko), $C4^{-/-}$ (c, n=10 mice in each group), $C1q^{-/-}$ (d, n=7 wt, n= 8 ko), $fB^{-/-}$ (e, n=9 wt, n=12 ko), $C5aR1^{-/-}$ (f, n=10 wt, n=19 ko), $C5aR2^{-/-}$ (g, n=14 wt, n=10 ko) and $C3aR^{-/-}$ (h, n=14 wt, n=16 ko) mice. One representative experiment out of three (a), two (b, d, e and f) or one (c, g and h) performed is shown. Experiment of panel d was performed using wt littermates. Exact p values are reported, two-tailed Wilcoxon matched-pairs signed rank test.

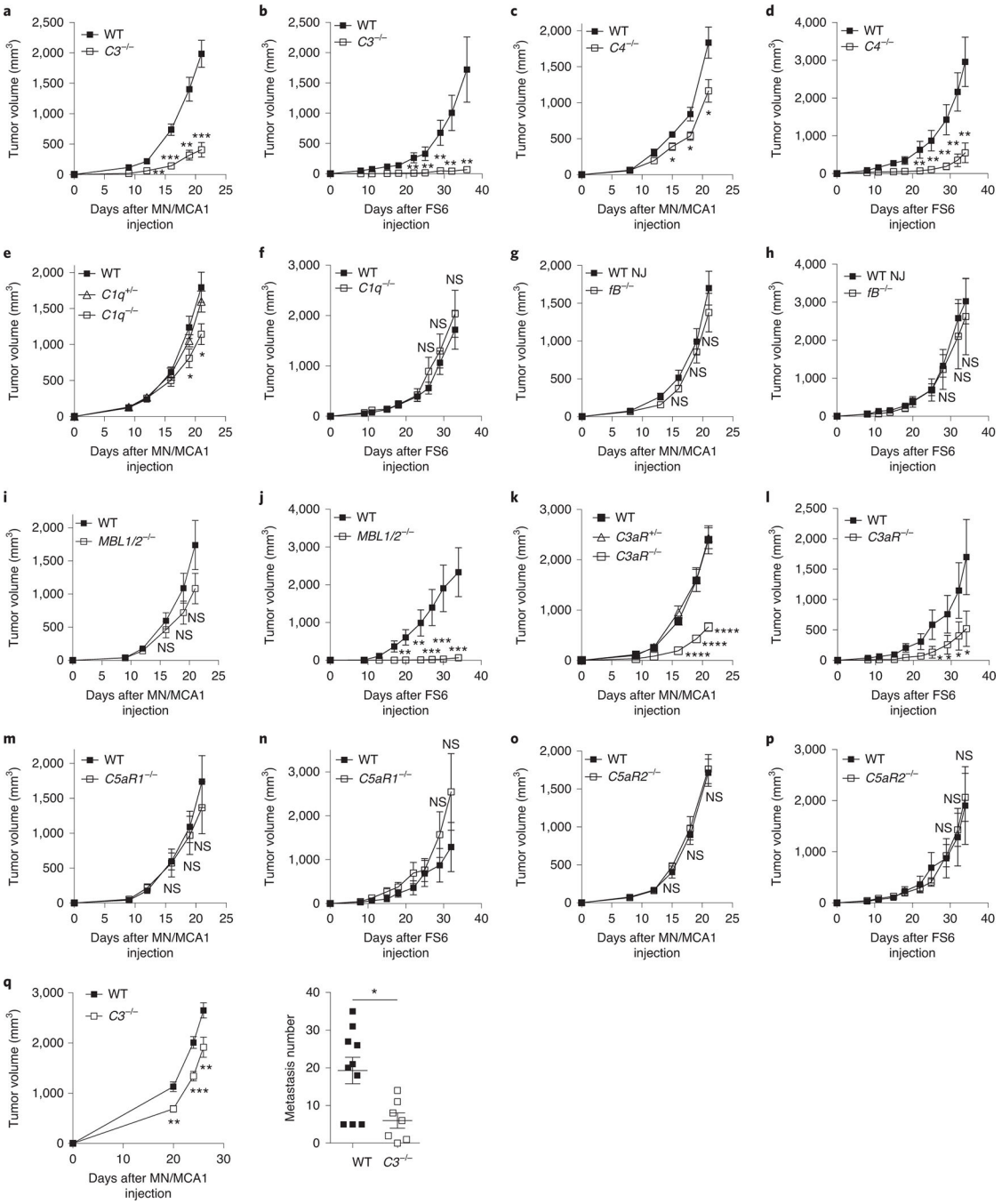

Figure 2. The lectin pathway and the C3aR promote transplanted sarcoma growth

(a-p) MN/MCA1 and FS6 tumor volumes (mean ± SEM) in *C3*$^{-/-}$ (a, n=5 mice in each group) and (b, n=14 wt, n=8 ko); *C4*$^{-/-}$ (c, n=10 wt, n=9 ko) and (d, n=11 wt, n=10 ko); *C1q*$^{-/-}$ (e, n=9 mice in each group) and (f, n=15 wt, n=8 ko); *fB*$^{-/-}$ (g, n=6 wt; n=4 ko) and (h, n=9 wt, n=4 ko); *MBL1/2*$^{-/-}$ (i, n=7 mice in each group) and (j, n=10 wt, n=9 ko); *C3aR*$^{-/-}$ (k, n=9 wt, n=9 he, n=8 ko) and (l, n=15 wt, n=12 ko); *C5aR1*$^{-/-}$ (m, n=7 wt, n=6 ko) and (n, n=12 wt, n=5 ko); *C5aR2*$^{-/-}$ (o, n=7 wt, n=4 ko) and (p, n=12 wt, n=8 ko) mice. (q) Primary tumor volume and number of lung metastasis 27 days after

MN/MCA1 tumor cell im injection in wt and *C3*$^{-/-}$ (mean ± SEM, n=10 wt, n=7 ko) mice. One representative experiment out of 15 (a), 8 (k), two (b, c, g, i, j, m and q) or one (d, f, n, o and p) performed is shown. e: Four pooled experiments performed with co-housed wt and heterozygous littermates. h, l: two pooled experiments. k: one out of 8 experiments was performed with co-housed littermates. The same wt mice were used simultaneously as control mice of experiments of panels i and m or for panels n, p and one out of the two pooled experiments of panel l. *p < 0.05, **p < 0.01, ***p < 0.001, ****p < 0.0001. Exact p values at the day of sacrifice are: a: p=0.0003; b: p=0.0014; c: p=0.025; d: p=0.0033; e: p=0.0218; j: p=0.0008; k: p<0.0001; l: p=0.0215; q left: p=0.0097; q right: p=0.0104. Unpaired two-tailed Student's t test (a: 16 and 21 days; c: 18 and 21 days; e; f; g; h; k: 16 days; m; o; q: 20 and 26 days) or two-tailed Mann Whitney test (a: 12 and 19 days; c: 15 days; d; i; j; k: 19 and 21 days; l; n; p; q: 24 days).

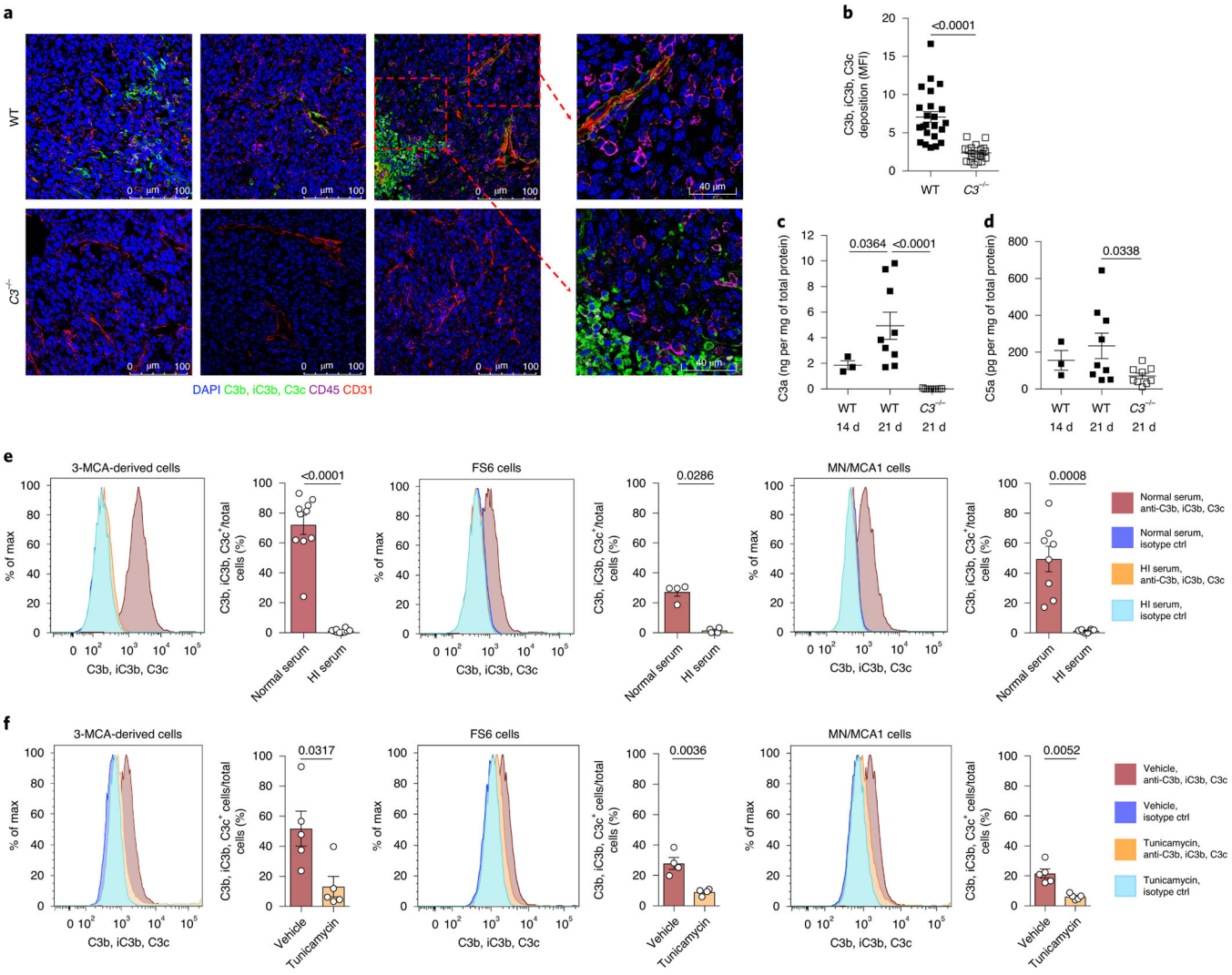

Figure 3. Complement deposition occurs on sarcoma cells

(a) Representative images of immunofluorescence analysis of C3 cleavage products (C3b, iC3b, C3c) deposition, vascular cells ($CD31^+$ cells) and immune cells ($CD45^+$ cells) in wt and $C3^{-/-}$-derived MN/MCA1 tumor tissues. Scale bar: 100μm. One out of two experiment performed (n=4 mice in each group), two-five or six fields have been acquired for each mouse in the two experiments. (b) Quantitation of C3 cleavage products (C3b, iC3b, C3c) deposition in wt and $C3^{-/-}$-derived tumor tissues (n=4 mice per group). Each dot represents the mean of fluorescence intensity (MFI) of one field; six fields have been acquired for each mouse. (c, d) Local C3a (c) and C5a (d) levels at different time points upon MN/MCA1 tumor cell injection in wt and $C3^{-/-}$ mice (n=3 wt mice at 14 days, n=9 wt mice at 21 days and 9 ko mice at 21 days). b-d: Mean ± SEM is shown. (e) Flow cytometric analysis of C3 deposition on 3-MCA-derived, FS6 and MN/MCA1 sarcoma cells incubated with heat inactivated (HI) or normal serum. Representative FACS plot (left panels) and quantification of C3b, iC3b, C3c-positive cells on total cells are shown (right panels) (n=10 independent experiments for one 3-MCA-derived cell line, n=4 independent experiments for FS6 cells, n=8 independent experiments for MN/MCA1 cells, mean ± SEM). (f) Flow cytometric

analysis of C3 deposition on sarcoma cells incubated with normal serum upon treatment with 10μg/ml tunicamycin or vehicle overnight. Representative FACS plots (left panels) and quantification of C3b, iC3b, C3c-positive cells (right panels) are shown (n=5 independent experiments for 3-MCA derived cells, n=4 independent experiments for FS6 cells, n=5 independent experiments for MN/MCA1 cells, mean ± SEM). Exact p values are reported. Unpaired two-tailed Student's t test (b; e; f: for MN/MCA1; d) or two-tailed Mann Whitney test (c; e; f: for 3-MCA1 and FS6).

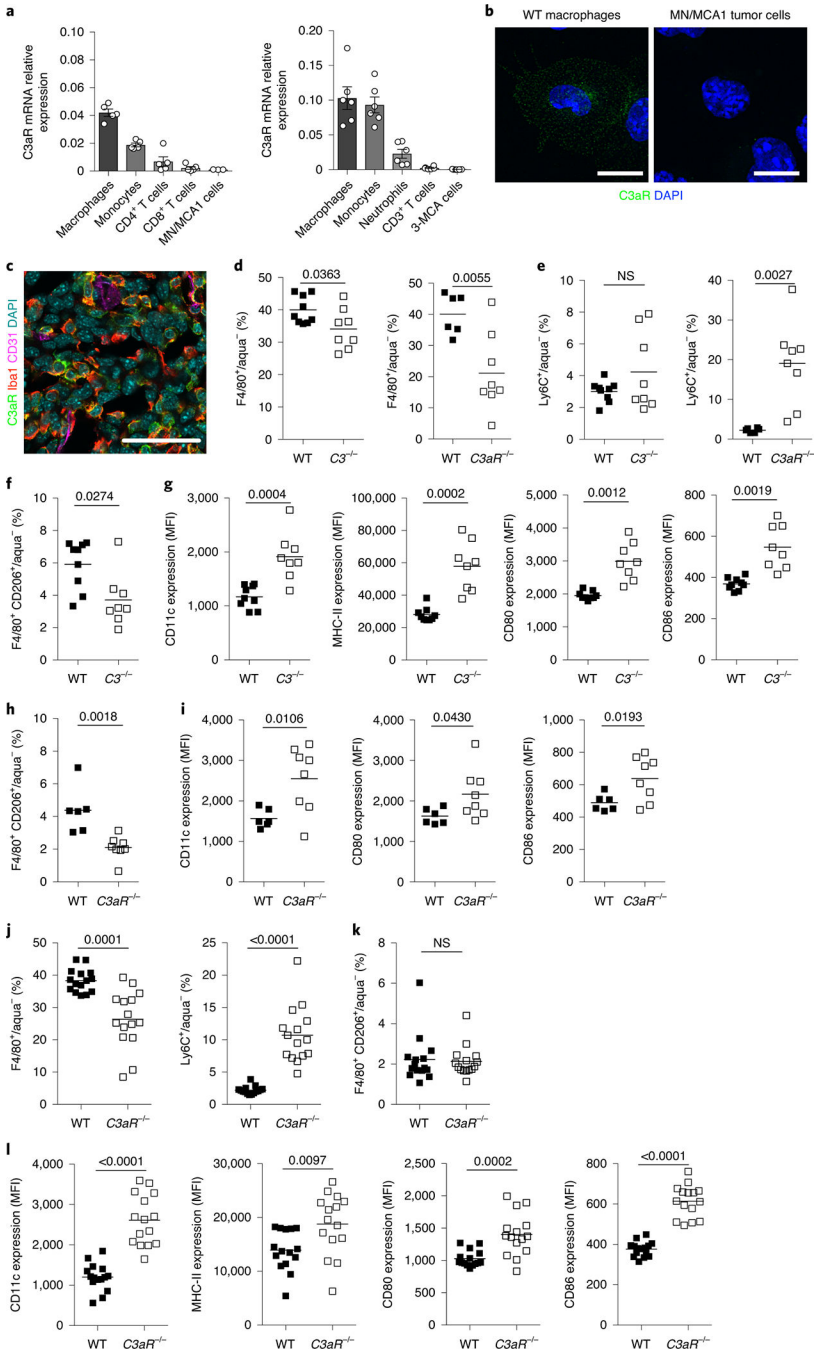

Figure 4. C3 and C3aR deficiency are associated with an M1-like TAM phenotype

(a) C3aR mRNA expression in MN/MCA1 (left panel) (n=3 independent experiments) or 3-MCA derived (right panel) (n=9 independent experiments) tumor cells and in leukocytes sorted from MN/MCA1 (left panel) or 3-MCA-induced (right panel) tumors of wt mice (n=5 or 6 mice; mean ± SEM). (b) Immunofluorescence analysis of C3aR expression in wt peritoneal macrophages, used as positive control, and MN/MCA1 tumor cells. One experiment performed with two technical replicates for each cell culture, two-three fields have been acquired for each replicate. Scale bar: 10μm. (c) Immunofluorescence analysis of

C3aR expression in tumor infiltrating macrophages (Iba-1+ cells) in wt derived MN/MCA1 tumor tissues. One experiment performed (n=5 mice), two-three fields have been acquired for each mouse. Scale bar: 50μm. (d, e) Analysis by FACS of macrophage (F4/80+) (d) and monocyte (Ly6C+) (e) frequency among living cells ($Aqua^{-}$) in MN/MCA1 tumors in wt and $C3^{-/-}$ (n=9 wt, n=8 ko) or $C3aR1^{-/-}$ (n=6 wt, n=8 ko) mice sacrificed 21 days after tumor cell injection. (f-i) Analysis by FACS of M2 macrophage frequency ($F4/80^{+}/CD206^{+}$) (f, h) and of the expression of selected M1 markers (CD11c, MHC II, CD80 and CD86) gated on total macrophages ($F4/80^{+}$) (g, i) in wt and $C3^{-/-}$ (f, g, n=9 wt, n=8 ko) or $C3aR^{-/-}$ (h, i, n=6 wt, n=8 ko) mice sacrificed 21 days after tumor cell injection. (j-l) Frequency of macrophages ($F4/80^{+}$) and monocytes ($Ly6C^{+}$) (j), M2 macrophages ($F4/80^{+}/CD206^{+}$) (k) and expression of M1 markers (CD11c, MHC II, CD80 and CD86) gated on total macrophages ($F4/80^{+}$) (l) in MN/MCA1 tumors in wt and $C3aR^{-/-}$ (n=15 in each group) mice sacrificed at similar tumor volume ($2cm^3$). d and e left panels, f and g: two experiments performed; d and e right panels, h and i: three experiments performed; j and l: one experiment performed. d-l: mean is shown. Exact p values are reported, unpaired two-tailed Student's t test (d; e; g: CD11c, CD80 and CD86 panels; h; i; j: $F4/80^{+}$ panel; l:CD11c, MHCII and CD86 panels) or two-tailed Mann Whitney test (f, g: MHCII panel; j: $Ly6C^{+}$ panel; k; l: CD80 panel).

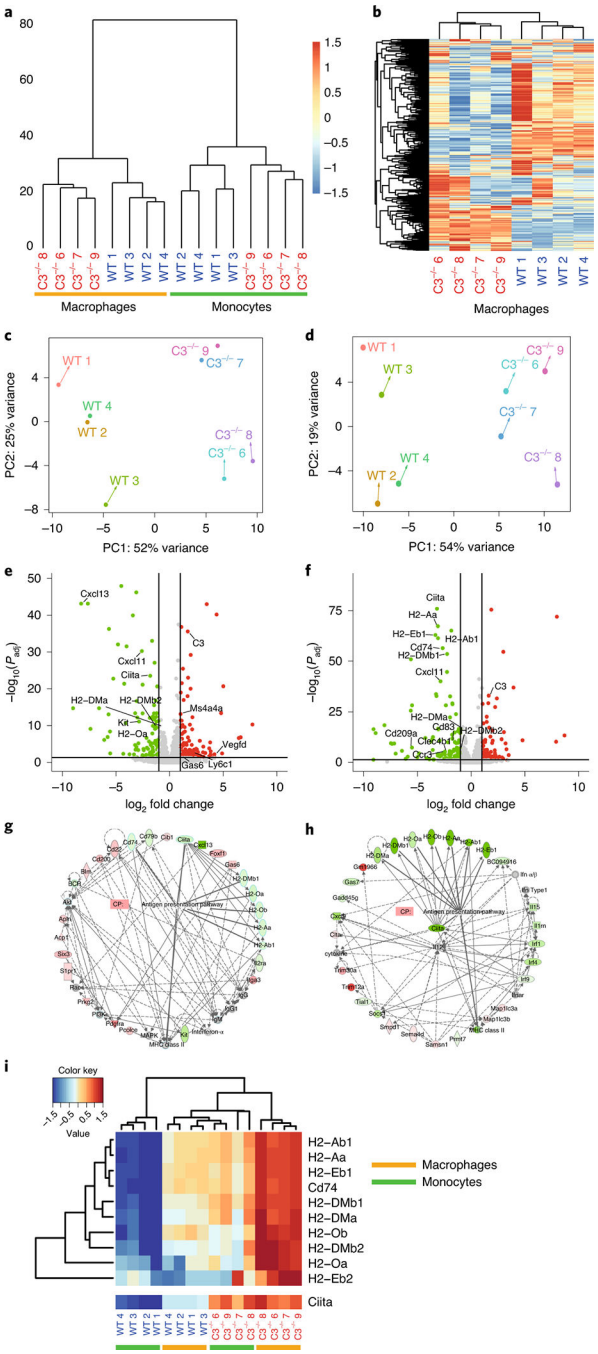

Figure 5. Transcriptional profile analysis of sarcoma infiltrating macrophages and monocytes

(a) Tree diagram for cluster analysis of FACS-sorted MN/MCA1 tumor-infiltrating macrophages and monocytes of wt (blue) and *C3*$^{-/-}$ (red) samples (n=4 mice per group). (b) Heatmap showing the first 1000 more differentially expressed genes in wt *vs C3*$^{-/-}$ macrophages. (c-d) Principal component (PC) analysis of RNA expression of macrophages (c) and monocytes (d). X and Y axes represent the first and the second PC, respectively. (e-f) Volcano plot showing differentially expressed genes (absolute log2FC > 1, adjusted p-value < 0.05) up-regulated (right) or down-regulated (left) in wt *vs C3*$^{-/-}$ macrophages (e)

and monocytes (f). Differential expression analyses are based on DESeq2 algorithm, which implies linear models fitting of the negative binomial distribution for each gene followed by two-sided Wald tests (null hypothesis of no difference between groups). Multiple experiment correction is applied within adjusted p-values. (g-h) Enrichment Functional Analysis using Ingenuity Pathway Analysis of differentially expressed genes (red: up-regulated, green: down-regulated) in wt *vs* $C3^{-/-}$ macrophages (g) and monocytes (h) showing modulation of MHC class II complex. The intensity of the color indicates the degree of up- or down-regulation. Solid or broken lines indicate direct or indirect relationship, respectively. (i) Heatmap representing the expression level of genes involved in the MHC class II complex pathway in wt (blue) versus $C3^{-/-}$ (red) macrophages and monocytes.

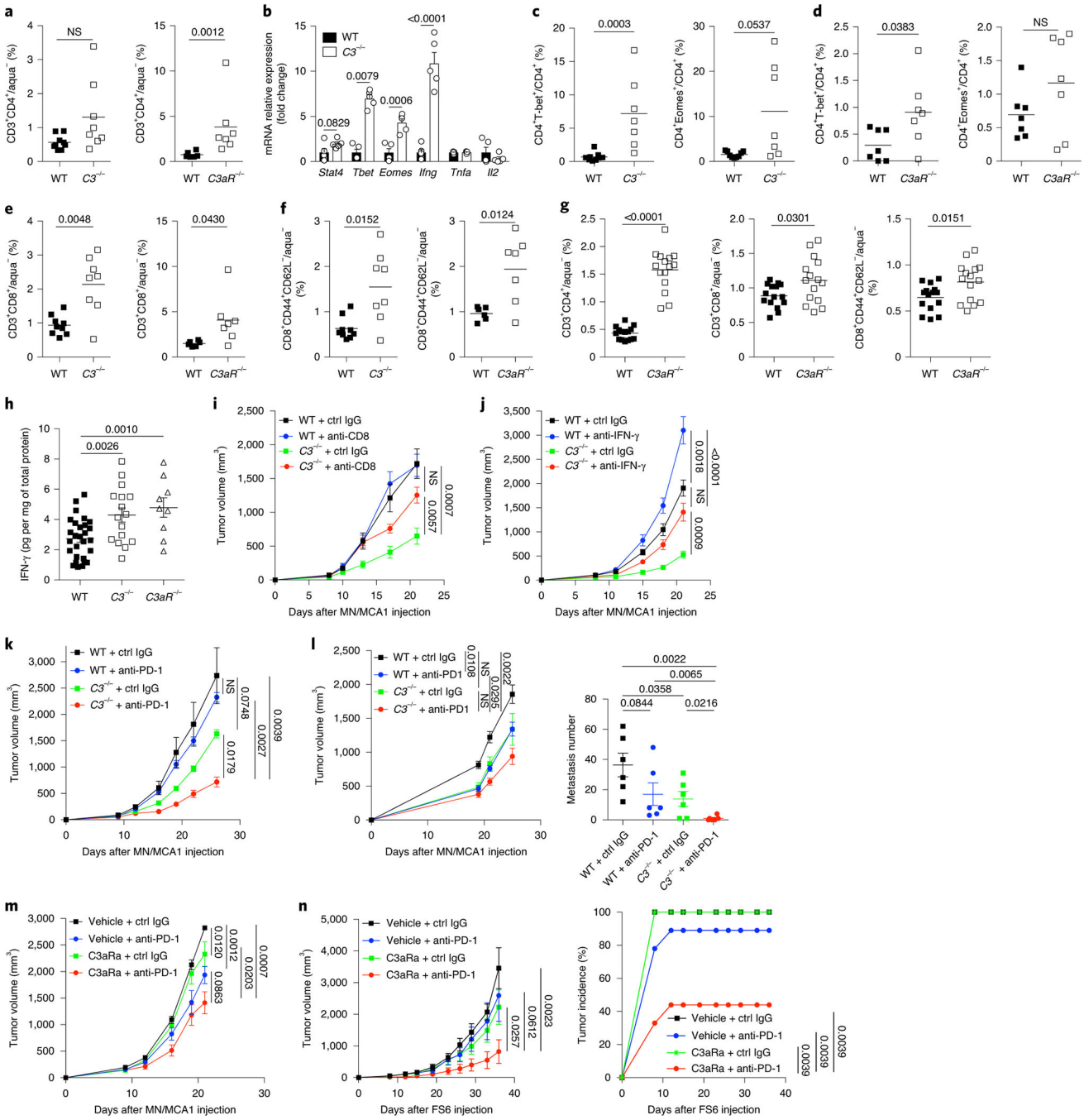

Figure 6. Effect of C3 and C3aR deficiency on T lymphocytes and response to immunotherapy

(a) FACS analysis of helper T cell ($CD3^+/CD4^+$) frequency in MN/MCA1 tumors (left, n=9 wt mice, n=8 *C3*$^{-/-}$ mice; right, n=6 wt mice, n=7 *C3aR*$^{-/-}$ mice). (b) Analysis by RT-PCR of selected Th1 markers of $CD4^+$ T cells sorted from MN/MCA1 tumors (mean ± SEM; n=5 mice per group). (c-e) Frequency of $CD4^+Tbet^+$ and $CD4^+Eomes^+$ (c, n=9 wt mice, n=7 *C3*$^{-/-}$ mice; d, n=7 mice in each group), $CD3^+CD8^+$ (e, left, n=9 wt mice, n=8 *C3*$^{-/-}$ mice; right, n=6 wt mice, n=7 *C3aR*$^{-/-}$ mice) and activated effector/effector memory T cells ($CD8^+CD44^+CD62L^-$) (f, left, n=9 wt mice, n=8 *C3*$^{-/-}$ mice; right, n=6 wt

mice, n=7 *C3aR*$^{-/-}$ mice) in MN/MCA1 tumors. (g) CD3^{+}CD4^{+}, CD3^{+}CD8^{+} and activated effector/effector memory T cell (CD8^{+}/CD44^{+}/CD62L^{-}) frequency in MN/MCA1 tumors of mice sacrificed at similar tumor volume (2cm^{3}) (n=15 mice in each group). a-g: mean is shown. (h) Local IFNγ in MN-MCA1 tumors (mean ± SEM; n=28 wt, n=16 *C3*$^{-/-}$, n=9 *C3aR*$^{-/-}$ mice from 4 pooled experiments). (i, j) MN/MCA1 primary tumor volume in mice treated with anti-CD8 (n=12 wt mice + ctrl IgG, n=9 wt mice + anti-CD8, n=11 ko mice + ctrl IgG, n=9 ko mice + anti-CD8) (i), anti-IFNγ (n=10 wt mice + ctrl IgG, n=10 wt or ko mice + anti- IFNγ, n=9 ko mice + ctrl IgG) (j) or ctrl IgG. (k) Primary tumor volume after MN/MCA1 sc injection in mice (n=9 mice in each group) treated with anti-PD-1 or ctrl IgG. (l) MN/MCA1 primary tumor volume and lung metastasis in mice treated with anti-PD-1 or ctrl IgG, (n=6 mice in each group). (m, n) Primary tumor volume after MN/MCA1 (n=6 mice vehicle + ctrl IgG, n=7 mice vehicle + anti-PD1, n=9 mice C3aRa + ctrl IgG, n=8 mice C3aRa + anti-PD1) (m) or FS6 (n=8 mice vehicle + ctrl IgG, n=9 mice vehicle or C3aRa + anti-PD1, n=8 mice C3aRa + ctrl IgG) (n) sc injection in wt mice treated with C3aRa or vehicle, and anti-PD-1 or ctrl IgG. i-n: mean ± SEM is shown. a, e and f left panels: three experiments performed; a, e and f right panels: four experiments performed; c, d: two experiments performed; b, g, j, k, l, m and n: one experiment performed; i: two pooled experiments. Exact p values are reported, unpaired two-tailed Student's t test (b: for *Stat4*, *Eomes*, *Ifng* and *Tnfa*; c: left panel; d; e; f: right panel; g; h) or two-tailed Mann Whitney test (a; b: for *Tbet* and *Il2*; c: right panel; f: left panel), Kruskal Wallis [p=0.0008 (i), p=0.0042 (k), p=0.0111 (l left panel), p=0.0033 (l right panel), p=0.0009 (m) and p=0.0194 (n left panel)] or Ordinary one-way Anova (p<0.0001) (j) with unpaired two-tailed Student's t test or two-tailed Mann Whitney U-test as *post-hoc* tests (i-n) and two-tailed Wilcoxon matched-pairs signed rank test (n, right panel).

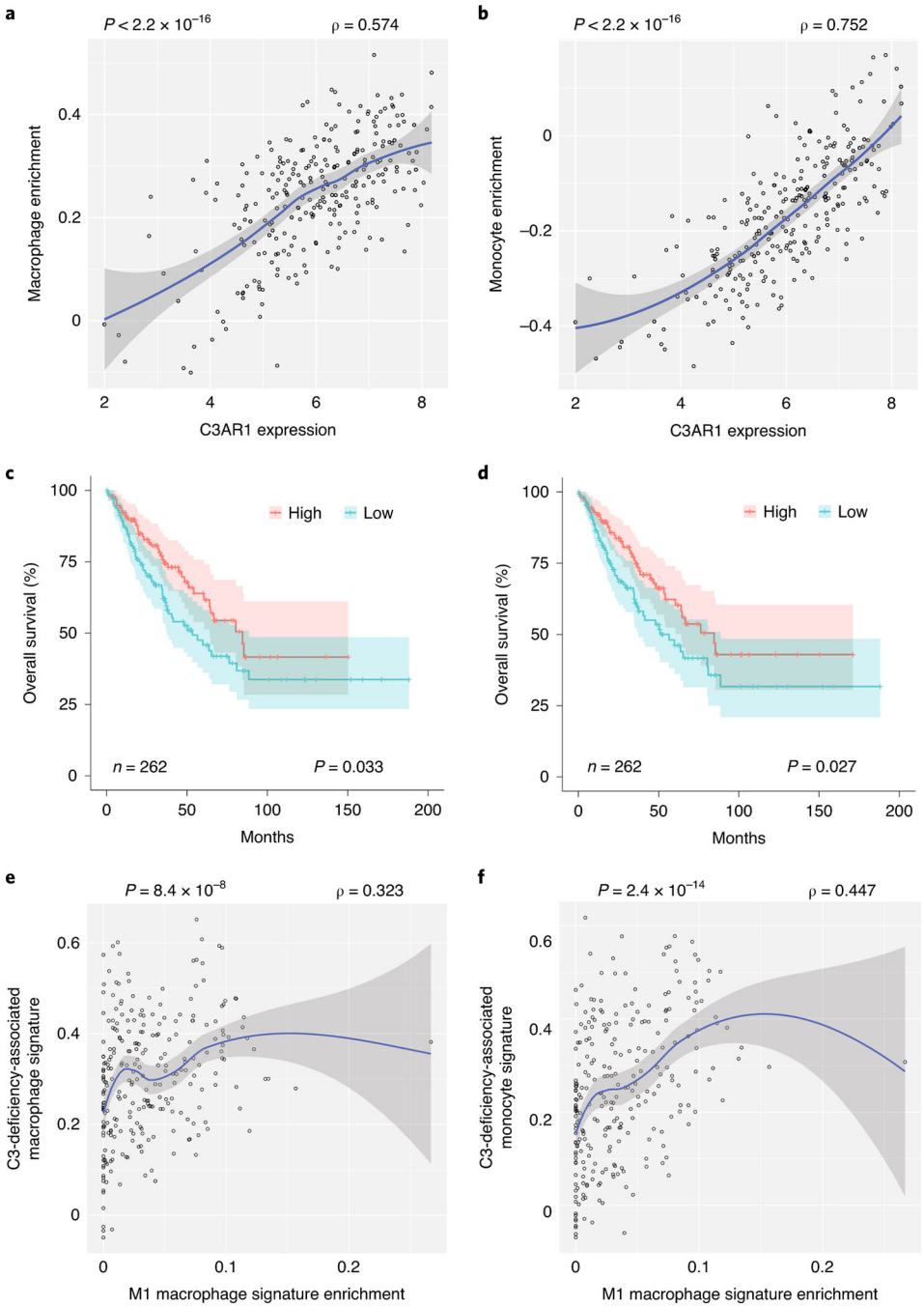

Figure 7. Prognostic significance of C3 deficiency-associated signatures in sarcoma patients

(a-b) Correlation plot between C3AR1 expression level and macrophage (a) or monocyte (b) quantification scores. Blue line: linear model interpolating curve; darker bands: linear model confidence intervals (n = 263 patients). (c-d) Kaplan-Meier survival curves of TCGA sarcoma patients divided based on the median enrichment scores of C3 deficiency-associated signatures of macrophages (n=60 increasing genes) (c) and monocytes (n=85 increasing genes) (d) (n=262 patients in total, n = 131 patients in each group, the patient corresponding to the median value has been excluded by the analysis). Shaded areas of Kaplan-Meier

survival curves represent 95% upper and lower confidence intervals. (e-f) Correlation plot between C3 deficiency-associated signature of macrophages (e) or monocytes (f) and a M1-like macrophage signature (n=263 patients). Blue line: linear model interpolating curve; darker bands: linear model confidence intervals. (a-f) Exact p value of two-sided Log-rank test (for survival curves) and correlation test (Spearman correlation for scatterplots) are reported.